Supporting Information

For

A Homoleptic Ag^{III} Complex Stabilized by Succinimidate Ligands

Emil Mickey Hilligsøe Larsen,[a] Theis Brock-Nannestad,[a] Jørgen Skibsted,[b] Anders Reinholdt,[a,c,*] Jesper Bendix[a,*]

[a] *Department of Chemistry*
University of Copenhagen
Universitetsparken 5, DK-2100 Copenhagen (Denmark)
Email: bendix@kiku.dk

[b] *Department of Chemistry and Interdisciplinary Nanoscience Center (iNANO)*
Aarhus University
Langelandsgade 140, DK-8000 Aarhus C (Denmark)

[c] *Department of Chemistry, Lund University*
P. O. Box 124, 22100 Lund, Sweden
Email: anders.reinholdt@chem.lu.se

1: Contents

1: Contents **S2**

2: Materials and Experimental Methods **S4**

3: Synthetic Procedures **S7**

3.1: Synthesis of $Cs[Ag(succ)_4] \cdot 4\ H_2O$ (**2**^{Cs}) S7

3.2: Generation of $Cs[Ag(succ)_2] \cdot 4\ H_2O$ (**1**^{Cs}) from **2**^{Cs} in water S9

3.3: Synthesis of $Rb[Ag(succ)_4] \cdot 4\ H_2O$ (**2**^{Rb}) S9

3.4: Synthesis of $K[Ag(succ)_4] \cdot 4\ H_2O$ (**2**^{K}) S10

3.5: Synthesis of $[(H_2O)Ag][Ag(succ)_4] \cdot 4\ H_2O$ (**2**^{Ag}) S10

3.6: Synthesis of $[(H_2O)Na]_2[Pd(succ)_4]$ (**3**^{Na}) S11

4: IR Spectroscopy **S13**

4.1: IR Spectral Data for $Cs[Ag(succ)_4] \cdot 4\ H_2O$ (**2**^{Cs}) S13

4.2: IR Spectral Data for $Rb[Ag(succ)_4] \cdot 4\ H_2O$ (**2**^{Rb}) S14

4.3: IR Spectral Data for $K[Ag(succ)_4] \cdot 4\ H_2O$ (**2**^{K}) S14

4.4: IR Spectral Data for $[(H_2O)Ag][Ag(succ)_4] \cdot 4\ H_2O$ (**2**^{Ag}) S15

4.5: IR Spectral Data for $[(H_2O)Na]_2[Pd(succ)_4]$ (**3**^{Na}) S15

5: NMR Spectroscopy on Samples in Solution **S16**

5.1: NMR Spectral Data for $Cs[Ag(succ)_4] \cdot 4\ H_2O$ (**2**^{Cs}) S16

5.2: NMR Spectral Data for $[(H_2O)Na]_2[Pd(succ)_4]$ (**3**^{Na}) S17

6: UV-vis Spectroscopy **S18**

6.1: UV-vis Spectral Data for $Cs[Ag(succ)_4] \cdot 4\ H_2O$ (**2**^{Cs}) S18

6.2: UV-vis Spectral Data for $[(H_2O)Ag][Ag(succ)_4] \cdot 4\ H_2O$ (**2**^{Ag}) S18

6.3: UV-vis Spectral Data for **2**^{Cs} and **2**^{Ag} in H_2O (Overlay) S19

6.4: UV-vis Spectral Data for **2**^{Cs} and **2**^{Ag} in solid KBr (Overlay) S19

6.5: UV-vis Spectral Data for $[(H_2O)Na]_2[Pd(succ)_4]$ (**3**^{Na}) S20

6.6: UV-vis Spectral Data for Na(succ) S20

7: Kinetic Studies of Decomposition of 2^{Cs} in Aqueous Solution **S21**

8: Mass Spectrometry **S24**

8.1: Mass Spectrometric Data for $Cs[Ag(succ)_4] \cdot 4\ H_2O$ (**2**^{Cs}) S24

8.2: Mass Spectrometric Data for $[(H_2O)Na]_2[Pd(succ)_4]$ (**3**^{Na}) S28

9: Single Crystal X-ray Diffraction **S32**

9.1 Crystallographic Tables S32
9.2 Thermal Ellipsoid Plots S35
Figure S28. $Rb[Ag(succ)_4] \cdot 4\ H_2O$ (**2^{Rb}**) S35
Figure S29. $K[Ag(succ)_4] \cdot 4\ H_2O$ (**2^{K}**) S35
Figure S30. $[(H_2O)Na]_2[Pd(succ)_4] \cdot 2\ H_2O$ (**3Na**) S36
Figure S31. $Cs[Ag(succ)_2] \cdot 4\ H_2O$ (**1^{Cs}**) S36
10: Powder X-ray Diffraction S37
11: Magnetic Measurements S38
12: Computational modeling S39
13: References S41

2: Materials and Experimental Methods

Starting materials, $AgNO_3$, Cs_2SO_4 (Fluka, >98%), Rb_2SO_4 (Merck, Suprapur®), D_2O (Sigma, 99.9% D), $HClO_4$ (FERAK, 70%), KOH pellets (Sigma-Aldrich, ≥85%), NaOH granules (Chemsolute, min. 98.8%), NaOH pellets (Sigma-Aldrich, ≥98%), $Na_2[S_2O_8]$, $K_2[S_2O_8]$ (Riedel-de Haën®, extra pure), $PdCl_2$ (Fluka, purum), and succinimide (Hsucc, Sigma-Aldrich) were purchased from commercial suppliers and used as received. Na(succ) was generated by dissolving equimolar amounts of NaOH and Hsucc in water.

IR spectra were recorded on solid samples using an Agilent Technologies Cary 630 FTIR instrument in total attenuated reflection mode (ATR).

NMR spectra of samples in solution were recorded using a 500 MHz Bruker instrument with a broad-band probe (^{1}H NMR) or a 500 MHz Bruker instrument with a cryoprobe ($^{13}C\{^1H\}$ NMR). For ^{1}H NMR spectra, residual solvent signals were used for calibration (D_2O: ^{1}H at 4.79 ppm). For ^{13}C NMR spectra, a capillary containing MeOH in D_2O was used for calibration (MeOH: ^{13}C at 49.50 ppm).[1]

Solid-state ^{109}Ag MAS NMR spectra were acquired at 14.09 T (27.9 MHz for ^{109}Ag) on a Varian Direct-Drive spectrometer using a home-built 5 mm CP/MAS NMR probe. The single-pulse spectra employed a 45° pulse (6 μs) for an rf field strength of $\gamma B_1/2\pi$ = 21 kHz and relaxation delays of 180 – 600 s. ^{109}Ag chemical shifts are relative to a 1.0 M $AgNO_3$ solution at 21 °C. The actual sample temperatures were determined using ^{207}Pb MAS NMR of $Pb(NO_3)_2$ as a NMR thermometer[2] from separate ^{207}Pb NMR spectra acquired under the same experimental conditions. The simulations considered the first-order chemical shift interaction and were conducted using the *STARS* software.[3]

UV-vis absorption spectra were recorded using a Perkin Elmer Lambda 2 spectrometer equipped with a 1 cm quartz cuvette. For kinetic studies, spectra were recorded at 2 or 5 minute intervals, depending on the decomposition rate. For solid-state UV-vis spectra, samples of $\mathbf{2^{Cs}}$ (7.7 mg) and $\mathbf{2^{Ag}}$ (7.6 mg) were ground with 4.00 g KBr in a mortar, and 80 mg of these mixtures were pressed into a pellet (diameter 1.0 cm) by applying a pressure of 15-20 tons.

Mass spectra were recorded using a Bruker Solarix XR ESI/MALDI FT-ICR MS instrument (ESI^-).

Elemental analyses were carried out by the microanalytical services of the Department of Chemistry, University of Copenhagen using a FlashEA 1112 instrument.

X-ray crystallographic studies were carried out on single crystals, which were coated with mineral oil, mounted on nylon loops, and transferred to the nitrogen cold stream of the diffractometer. The single-crystal X-ray diffraction studies were performed on a Bruker D8 VENTURE diffractometer equipped with a Mo K_α high-brilliance IμS radiation source (λ = 0.71073 Å), a multilayer X-ray mirror and a PHOTON 100 CMOS detector, and an Oxford Cryosystems low temperature device. The instrument was controlled with the APEX2/APEX3 software package using SAINT.[4] Final cell constants were obtained from least squares fits of several thousand strong reflections. Intensity data were corrected for absorption using intensities of redundant reflections with the program SADABS.[5] The structures were solved in Olex2 using the olex2.solve[6] program (Charge Flipping) and refined using SHELXL.[7] Non-hydrogen atoms were refined anisotropically; in disordered fragments, the least occupant parts were refined isotropically, if necessary. CH_2 hydrogens were placed at calculated positions and refined as riding atoms. H_2O hydrogens were located in the difference Fourier maps and refined positionally (except for the least occupant parts of disordered H_2O, which were placed at calculated positions and refined as riding atoms). Isotropic displacement parameters were set to U_{iso} = 1.2 U_{eq} of the parent atom for both CH_2 and H_2O. Crystallographic details are listed in **Tables S1–S3**.

CCDC entries 2365916-2365920, and 2372376 contain the crystallographic data reported herein. These data can be obtained free of charge from The Cambridge Crystallographic Data Centre *via* www.ccdc.cam.ac.uk/data_request/cif.

Powder X-ray diffraction data were recorded at room temperature using a Bruker D8 ADVANCE powder diffractometer operating in a 2θ-θ configuration using Cu K_α radiation (λ = 1.5418 Å). Samples were ground and adhered onto double sided Kapton tape fastened on a poly(methyl methacrylate) sample holder. The powder patterns were simulated in Mercury with inclusion of preferred orientation effects (March-Dollase parameter = 0.5).

Magnetic measurements were recorded using a MPMS-XL SQUID magnetometer equipped with a 5 T dc magnet. The measurements were performed on a polycrystalline sample of $Cs[Ag(succ)_4] \cdot 4\ H_2O$ (**2**^{Cs}). The susceptibilities were corrected for diamagnetic contributions from the sample holder and the constituent atoms by means of Pascal's constants.

3: Synthetic Procedures

3.1: Synthesis of $Cs[Ag(succ)_4] \cdot 4\ H_2O$ ($\mathbf{2^{Cs}}$)

Method 1. Succinimide (Hsucc, 1.1 g, 11 mmol) was suspended in 2 ml water and dissolved by slowly adding 4 pellets of KOH (370 mg, 6.6 mmol). $AgNO_3$ (191 mg, 1.12 mmol) was dissolved in this succinimide buffer, resulting in a clear colorless solution. $Na_2[S_2O_8]$ (400 mg, 1.7 mmol) was added, and the solution was heated periodically over a gas flame over five minutes (gently, without boiling), attaining a yellow color ($[Ag(succ)_4]^-$). Cs_2SO_4 (1.0 g, 2.8 mmol; i.e. 5.5 mmol Cs^+) was added, and heating of the suspension (white precipitate) was maintained over five minutes. During heating, the precipitate attained a yellow color. Upon increasing the volume to 10 ml and heating, most of the precipitate dissolved, leaving small yellow crystals of $Cs[Ag(succ)_4] \cdot 4\ H_2O$ ($\mathbf{2^{Cs}}$) in the yellow solution. After 3 days, crystallization was complete (colorless mother liquor), and large yellow crystals of $\mathbf{2^{Cs}}$ were isolated by filtration, washed with ice water (3 × 10 ml) and dried on the filter frit using a water aspirator. Yield of $Cs[Ag(succ)_4] \cdot 4\ H_2O$ ($\mathbf{2^{Cs}}$): 427 mg, 0.606 mmol, 53.9% based on $AgNO_3$.

Method 2. Succinimide (Hsucc, 1.1 g, 11 mmol) was suspended in 4 ml water and dissolved by slowly adding 3 pellets of NaOH (300 mg, 7.5 mmol). $AgNO_3$ (240 mg, 1.41 mmol) was dissolved in this succinimide buffer, rapidly producing a precipitate of long colorless needle crystals of $Na[Ag(succ)_2]$. $Na_2[S_2O_8]$ (0.65 g, 2.7 mmol) was added, and the suspension was heated periodically over a gas flame for five minutes (gently, without boiling), resulting in a clear yellow solution ($[Ag(succ)_4]^-$). The solution was diluted to 10 ml, and Cs_2SO_4 (0.92 g, 2.5 mmol; i.e. 5.1 mmol Cs^+) was added, resulting in a less intense yellow color. Upon cooling, colorless needle crystals started depositing within 30-60 minutes. The suspension was again heated gently and diluted to 20 ml, slowly depositing small yellow crystals of $Cs[Ag(succ)_4] \cdot 4\ H_2O$ ($\mathbf{2^{Cs}}$) in the yellow solution. After 3 days, crystallization was complete (colorless mother liquor), and large yellow crystals of $\mathbf{2^{Cs}}$ were isolated by filtration, washed with ice water (3 × 10 ml) and dried on the filter frit using a water aspirator. Yield of $Cs[Ag(succ)_4] \cdot 4\ H_2O$ ($\mathbf{2^{Cs}}$): 539 mg, 0.764 mmol, 54.1% based on $AgNO_3$.

Comments on Methods 1 and 2: KOH and NaOH should be added slowly when generating the succinimide buffers to prevent hydrolysis of the imide (as evident from the

smell of ammonia). The crystallization of $\mathbf{2^{Cs}}$ proceeds slowly; completion typically requires days. Initially, the oxidation with $Na_2[S_2O_8]$ requires heating, but the solution must not boil; this results in rapid loss of the yellow color ($[Ag(succ)_4]^-$), continued liberation of oxygen, and formation of a turbidity (initially colorless, brown or black over days). When isolating the mother liquor (**Methods 1** and **2**) by filtration and adding a 1 M aqueous solution of NaCl, a white precipitate of AgCl (s) forms within seconds, demonstrating the presence of unreacted Ag^I species.

Method 3. A three-chamber diffusion cell (connected *via* glass frits) was fitted with a silver electrode (cathode, left chamber) and a platinum electrode (anode, 8 cm^2 surface area, middle chamber). The left chamber was charged with $AgNO_3$ (200 mg, 1.2 mmol) dissolved in 10 ml water. The middle chamber was charged with $AgNO_3$ (200 mg, 1.2 mmol), succinimide (1.1 g, 11 mmol), and 4 KOH pellets (360 mg, 6.4 mmol) dissolved in 10 ml water. The right chamber was charged with 10 ml of water. Upon adjusting the potential between the left and middle chambers to +0.80 V, the solution around the platinum electrode immediately attained a yellow color ($[Ag(succ)_4]^-$). Solid Cs_2SO_4 (0.50 g, 1.4 mmol; i.e. 2.8 mmol Cs^+) was then dissolved in the middle chamber, and upon standing overnight, yellow crystals of $Cs[Ag(succ)_4] \cdot 4\ H_2O$ (**2^{Cs}**) deposited on the Pt electrode. The electrode was rinsed with water, and air-dried overnight. The crystals of **2^{Cs}** were removed by scraping the electrode. Yield of $Cs[Ag(succ)_4] \cdot 4\ H_2O$ (**2^{Cs}**): 10 mg, 0.014 mmol, 1.2% based on $AgNO_3$. Following the above procedure with a potential of 1.20 V results in a yield of 16 mg **2^{Cs}** (0.023 mmol, 1.9% based on $AgNO_3$).

Comments on Method 3: The electrochemical oxidation affording **2^{Cs}** can readily be carried out in a two-chamber cell without a spectator compartment (the right chamber, filled with water). The oxidation process commences more rapidly at potentials exceeding ~1.0 V than is the case at 0.8 V. The low yield is a result of the limited surface area of the electrode (the cover of **2^{Cs}** crystals eventually prevents oxidation).

Characterization data for 2^{Cs}: IR (solid ATR, $\tilde{\nu}$/cm^{-1}): 1654, 1703 (C=O). **^{1}H NMR**, 500 MHz, D_2O, δ (ppm): 2.78 (s, 16H). **^{13}C NMR**, 126 MHz, D_2O, δ (ppm): 187.37, 31.33. **UV-vis**, H_2O, λ_{max} [nm, ε (M^{-1} cm^{-1})]: 222 (19400, inflection point), 302 (8100), 361 (4300, inflection point). **ESI-MS**, H_2O, [isotope cluster] calculated / found: $[Ag(succ)_4]^-$ 499.00; 501.00 / 499.02; 501.02, $[Cs\{Ag(succ)_4\}_2]^-$ 1132.91 / 1132.96, $[Cs_2\{Ag(succ)_4\}_3]^-$ 1764.82; 1766.82 / 1764.91; 1766.91. **Elemental analysis**, calculated

for $C_{16}H_{16}AgCsN_4O_8 \cdot 4\ H_2O$: C: 27.25%, H: 3.43%, N: 7.95%; found: C: 27.03%; H: 3.48%, N: 7.97%.

3.2: Generation of $Cs[Ag(succ)_2] \cdot 4\ H_2O$ ($\mathbf{1^{Cs}}$) from $\mathbf{2^{Cs}}$ in water

$Cs[Ag(succ)_4] \cdot 4\ H_2O$ ($\mathbf{2^{Cs}}$, 10 mg, 14 µmol) was dissolved in 2 ml water (yellow solution) and left standing for several days (closed), resulting in a colorless solution. The solution was allowed to evaporate overnight, leaving crystals of $Cs[Ag(succ)_2] \cdot 4\ H_2O$ (identified by X-ray crystallography). The residue was extracted with acetonitrile overnight, and by concentrating the acetonitrile extracts, crystalline Hsucc was isolated and identified by its ^1H NMR spectrum ($CDCl_3$) and X-ray crystallography [unit cell data conform with a published succinimide structure:[8] *Pbca*, a = 7.3379(4) Å, b = 9.5437(6) Å, c = 12.8196(8) Å, V = 897.8 Å^3 at 120(2) K].

3.3: Synthesis of $Rb[Ag(succ)_4] \cdot 4\ H_2O$ ($\mathbf{2^{Rb}}$)

Succinimide (Hsucc, 1.02 g, 10.3 mmol) was suspended in 10 ml water and dissolved by slowly adding 3 pellets of NaOH (293.5 mg, 7.34 mmol). $AgNO_3$ (233.3 mg, 1.37 mmol) was dissolved in this succinimide buffer, yielding a clear, colorless solution. $Na_2[S_2O_8]$ (0.62 g, 2.6 mmol) was added, resulting in precipitation of colorless needle crystals of $Na[Ag(succ)_2]$. The suspension was heated periodically using a heat gun (gently, without boiling), resulting in a clear yellow solution. Rb_2SO_4 (1.03 g, 3.85 mmol) was added, and heating was continued to dissolve the salt. Upon cooling, colorless needle crystals started depositing within 30-60 minutes. The suspension was again heated gently and diluted to 20 ml, slowly depositing small yellow crystals of $Rb[Ag(succ)_4] \cdot 4\ H_2O$ ($\mathbf{2^{Rb}}$) in the yellow solution. After 5 days, crystallization was complete (colorless mother liquor), and large yellow crystals of $\mathbf{2^{Rb}}$ were isolated by filtration, washed with water (3 × 10 ml) and dried on the filter frit using a water aspirator. Yield of $Rb[Ag(succ)_4] \cdot 4\ H_2O$ ($\mathbf{2^{Rb}}$): 407.1 mg, 0.619 mmol, 45.1% based on $AgNO_3$.

Characterization data for $\mathbf{2^{Rb}}$: IR (solid ATR, $\tilde{\nu}$/cm^{-1}): 1654, 1705 (C=O). **Elemental analysis**, calculated for $C_{16}H_{16}AgN_4O_8Rb \cdot 4\ H_2O$: C: 29.22%, H: 3.68%, N: 8.52%; found: C: 29.56%; H: 3.59%, N: 8.30%.

3.4: Synthesis of $K[Ag(succ)_4] \cdot 4\ H_2O$ ($\mathbf{2^K}$)

Succinimide (Hsucc, 1.14 g, 11.5 mmol) was suspended in 5 ml water and dissolved by slowly adding 5 pellets of KOH (516 mg, 9.20 mmol). $AgNO_3$ (376.4 mg, 2.22 mmol) was dissolved in this succinimide buffer, yielding a clear, colorless solution. $K_2[S_2O_8]$ (741 mg, 2.74 mmol) was added, and the solution was heated periodically using a heat gun (gently, without boiling), resulting in a clear yellow solution. Upon cooling, colorless needle crystals started depositing within 30-60 minutes. The suspension was again heated gently and diluted to 10 ml, slowly depositing small yellow crystals of $K[Ag(succ)_4] \cdot 4\ H_2O$ ($\mathbf{2^K}$) in the yellow solution. After 5 days, the solution remained yellow (due to the considerable solubility of $\mathbf{2^K}$); however, yellow crystals of $\mathbf{2^K}$ were deposited together with large (> 1 mm × 1 mm × 1 mm) colorless crystals of a by-product. The yellow crystals of $\mathbf{2^K}$ were removed from the colorless crystals using a pipette, collected on a filter frit, washed quickly with water (3 × 2 ml), and dried in a dynamic vacuum using a water aspirator. A few remaining colorless crystals were removed using a spatula. Yield of $K[Ag(succ)_4] \cdot 4\ H_2O$ ($\mathbf{2^K}$): 150.4 mg, 0.246 mmol, 11.1% based on $AgNO_3$.

Comments: The low yield of $\mathbf{2^K}$ reflects its relatively high solubility in water. Apart from the colorless by-product, the formation of $\mathbf{2^K}$ is frequently accompanied by a dark material (soluble in succinimide buffer), even when the reaction mixture is excluded from sunlight.

Characterization data for $\mathbf{2^K}$: IR (solid ATR, $\tilde{\nu}/cm^{-1}$): 1654, 1753 (C=O). **Elemental analysis**, calculated for $C_{16}H_{16}AgKN_4O_8 \cdot 4\ H_2O$: C: 31.43%, H: 3.96%, N: 9.16%; found: C: 31.48%; H: 3.59%, N: 8.89%.

3.5: Synthesis of $[(H_2O)Ag][Ag(succ)_4] \cdot 4\ H_2O$ ($\mathbf{2^{Ag}}$)

Succinimide (Hsucc, 1.09 g, 11.0 mmol) was suspended in 10 ml water, and 4 sodium hydroxide pellets (373 mg, 9.33 mmol) were added, resulting in dissolution of the solids. $AgNO_3$ (774 mg, 4.56 mmol) was added; initially the silver nitrate dissolved, followed by crystallization of colorless needle crystals of $Na[Ag(succ)_2]$, which were redissolved by heating the reaction flask with a heat gun. $Na_2[S_2O_8]$ (1.2 g, 5.0 mmol) was added, immediately resulting in a yellow color of the solution. The solution was kept warm with the heat gun, turning the reaction mixture into a clear orange solution and then left to slowly cool to room temperature. Over the course of five minutes, the solution turned

dark red, and dark yellow-orange crystals deposited alongside colorless crystals, while the solution bubbled vigorously. The colorless crystals were identified as Ag_2SO_4 based on their unit cell (X-ray diffraction), and could be removed by washing with succinimide buffer (prepared from 1.0 g Hsucc and 380 mg NaOH in 10 ml H_2O). When washing the mixture of dark orange crystals and colorless crystals (Ag_2SO_4) with 2 ml of the succinimide buffer, the colorless crystals dissolved leaving a pure sample of dark orange crystals of $[(H_2O)Ag][Ag(succ)_4] \cdot 4\ H_2O$ (**2^{Ag}**), which were collected on a filter frit, washed with water (3 × 2 ml), and dried in a dynamic vacuum. Yield of $[(H_2O)Ag][Ag(succ)_4] \cdot 4\ H_2O$ (**2^{Ag}**): 1071 mg, 1.53 mmol, 67.3% based on $AgNO_3$.

Comment: In this synthesis, sodium salts (NaOH, $Na_2[S_2O_8]$) are more suitable than potassium salts because the latter tend to favor formation of $K[Ag(succ)_4] \cdot 4\ H_2O$ (**2^{K}**).

Characterization data for 2^{Ag}: IR (solid ATR, $\tilde{\nu}$/cm^{-1}): 1648, 1753 (C=O). **UV-vis**, H_2O, λ_{max} [nm, ε (M^{-1} cm^{-1})]: 224 (22000, inflection point), 303 (11900), 362 (6400, inflection point). **Elemental analysis**, calculated for $C_{16}H_{18}Ag_2N_4O_9 \cdot 4\ H_2O$: C: 27.53%, H: 3.75%, N: 8.03%; found: C: 27.35%; H: 3.74%, N: 8.06%.

3.6: Synthesis of $[(H_2O)Na]_2[Pd(succ)_4]$ (3^{Na})

Succinimide (Hsucc, 0.80 g, 8.1 mmol) was suspended in 1 ml water, and sodium hydroxide granules (0.16 g, 4.0 mmol) were added in portions with 1 ml water, resulting in the dissolution of the solids. $PdCl_2$ (104 mg, 587 µmol) was added, and the solution was diluted to 4 ml and heated to reflux temperature until all $PdCl_2$ had dissolved and the volume had decreased to ca. 2 ml (ca. 10 minutes). During this process, white crystals of $[(H_2O)Na]_2[Pd(succ)_4] \cdot 2\ H_2O$ (**3^{Na}**) started separating. The reaction mixture was stored at 5 °C for one hour, and the crystals were separated by filtration, rinsed quickly with ice water, and dried at 100 °C for one hour, resulting in loss of 2 H_2O molecules from the product. Yield of $[(H_2O)Na]_2[Pd(succ)_4]$ (**3^{Na}**): 261 mg, 449 µmol, 76.6% based on $PdCl_2$.

Characterization data for 3^{Na}: IR (solid ATR, $\tilde{\nu}$/cm^{-1}): 1630, 1712 (C=O). **^{1}H NMR**, 500 MHz, D_2O, δ (ppm): 2.50 (s, 16H). **^{13}C NMR**, 126 MHz, D_2O, δ (ppm): 194.24, 31.00. **UV-vis**, H_2O, λ_{max} [nm, ε (M^{-1} cm^{-1})]: 216 (49100), 289 (290), 336 (120, inflection point). **ESI-MS**, H_2O, [isotope cluster] calculated / found: $[Pd(succ)_3]^-$ 399.98; 401.98 /

399.99; 401.99, $[Pd(succ)_3(H_2O)]^-$ 417.99; 419.99 / 418.00; 420.00, $[Na\{Pd(succ)_4\}]^-$ 520.99; 522.99 / 521.01;523.01. **Elemental analysis**, calculated for $C_{16}H_{20}N_4Na_2O_{10}Pd$: C: 33.09%, H: 3.47%, N: 9.65%; found: C: 33.40%, H: 3.55%, N: 9.54%.

4: IR Spectroscopy

4.1: IR Spectral Data for Cs[Ag(succ)$_4$] · 4 H_2O (2^{Cs})

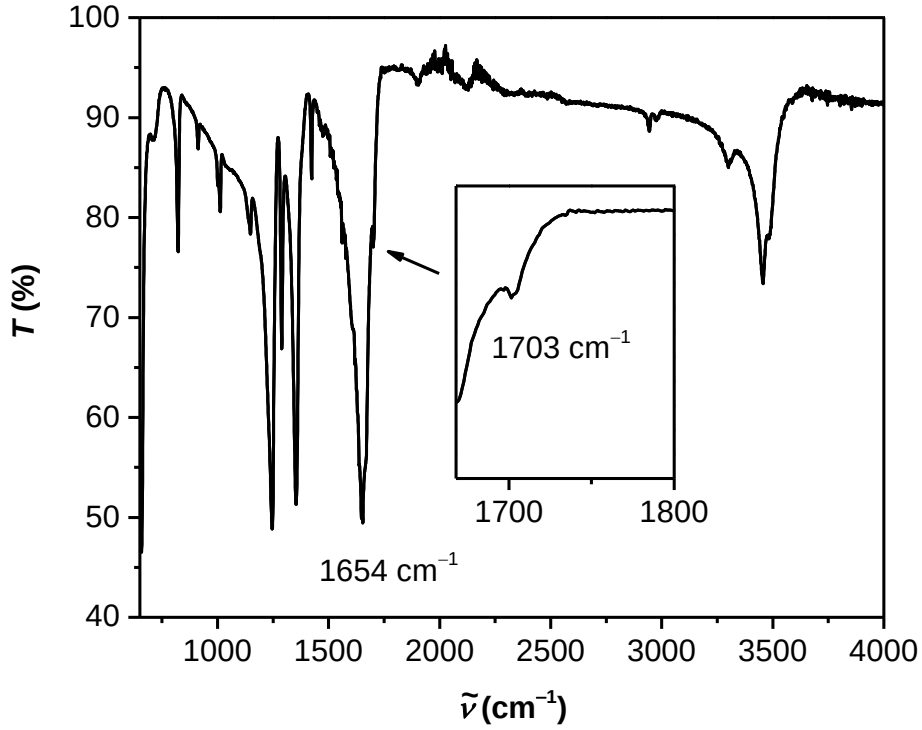

Figure S1. IR spectrum of crystalline **2^{Cs}**.

4.2: IR Spectral Data for Rb[Ag(succ)$_4$] · 4 H$_2$O (2^{Rb})

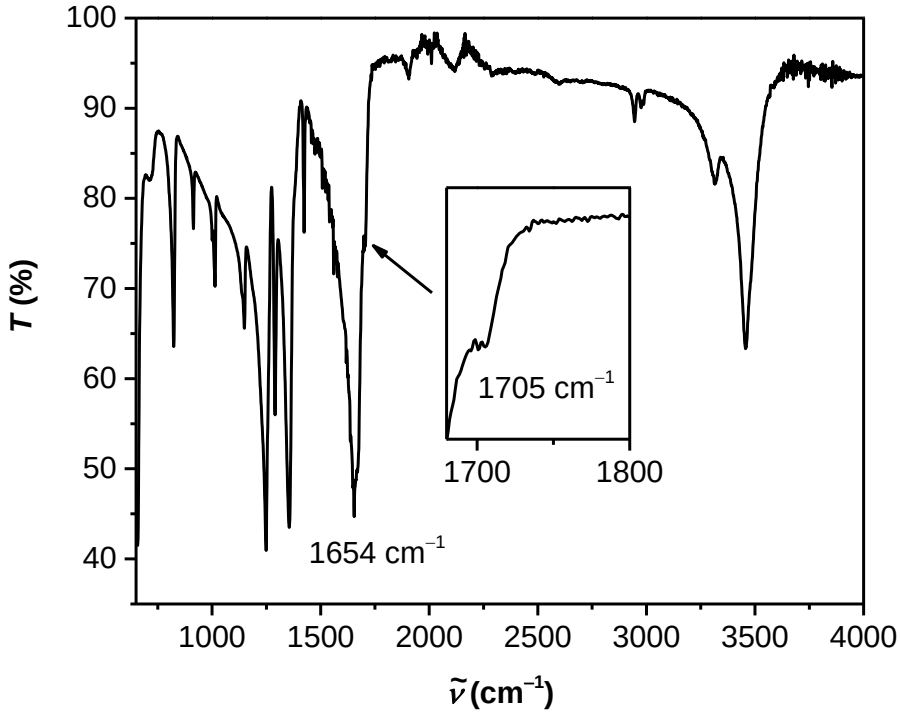

Figure S2. IR spectrum of crystalline **2^{Rb}**.

4.3: IR Spectral Data for K[Ag(succ)$_4$] · 4 H$_2$O (2^{K})

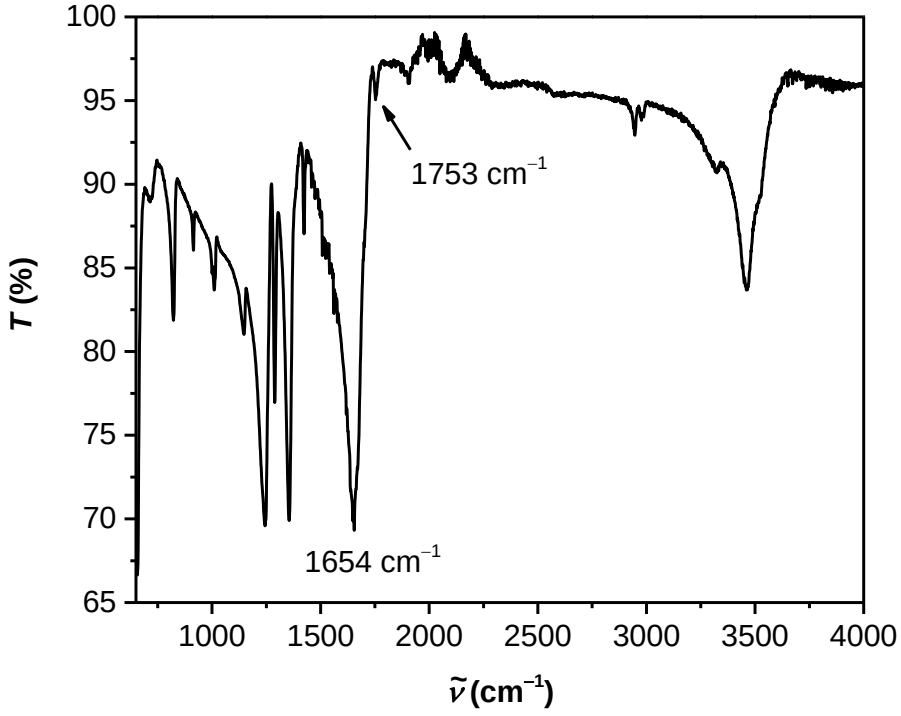

Figure S3. IR spectrum of crystalline **2^{K}**.

4.4: IR Spectral Data for $[(H_2O)Ag][Ag(succ)_4] \cdot 4\ H_2O$ (2^{Ag})

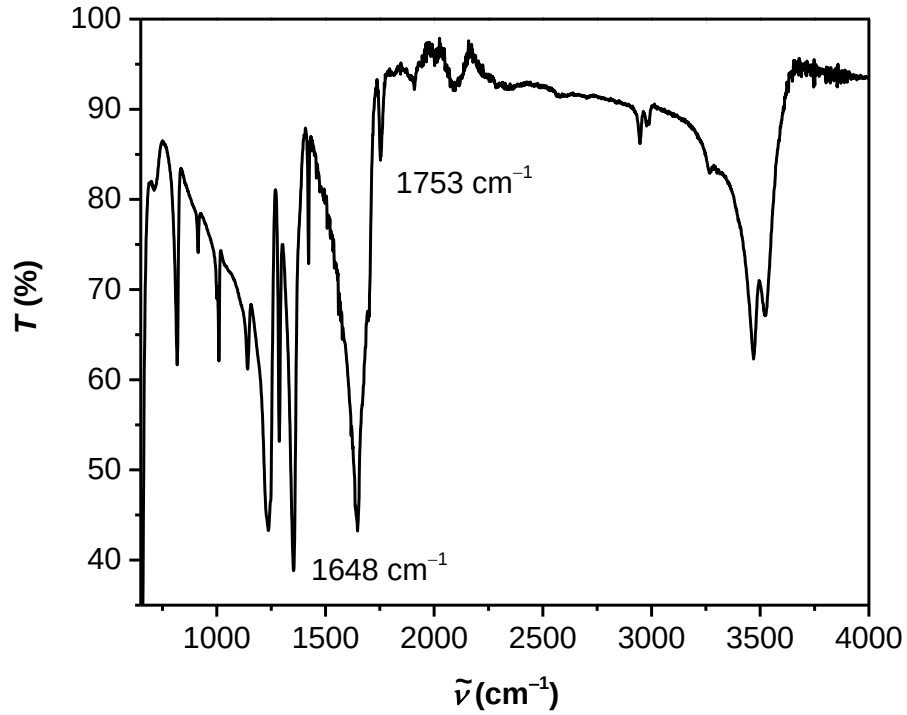

Figure S4. IR spectrum of crystalline $\mathbf{2^{Ag}}$.

4.5: IR Spectral Data for $[(H_2O)Na]_2[Pd(succ)_4]$ (3^{Na})

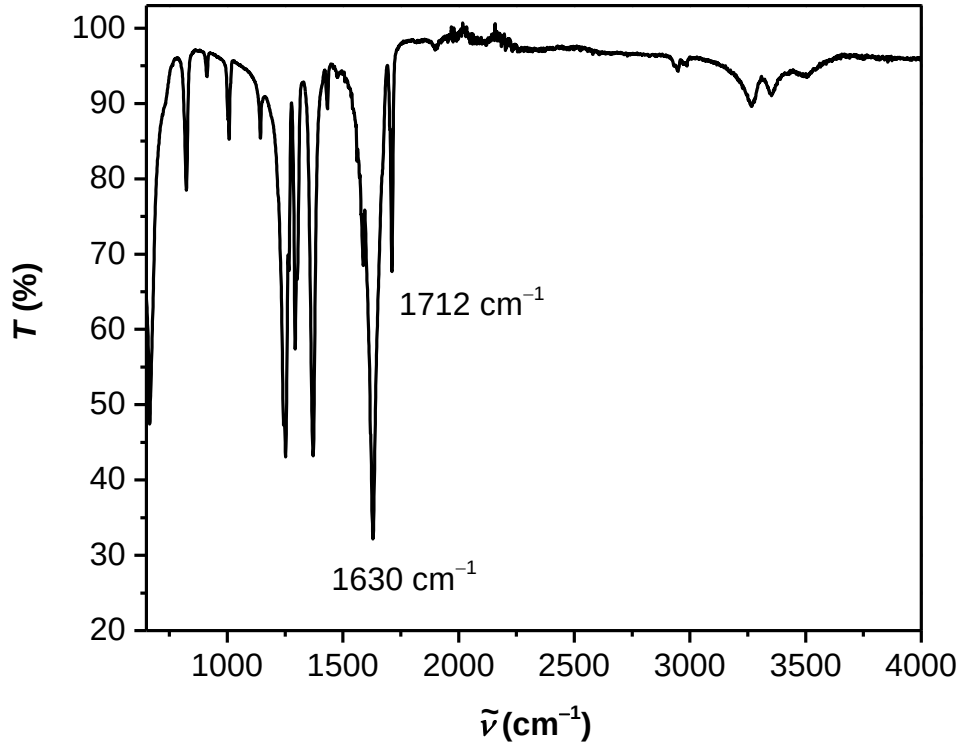

Figure S5. IR spectrum of crystalline $\mathbf{3^{Na}}$.

5: NMR Spectroscopy on Samples in Solution

5.1: NMR Spectral Data for $Cs[Ag(succ)_4] \cdot 4\ H_2O$ (2^{Cs})

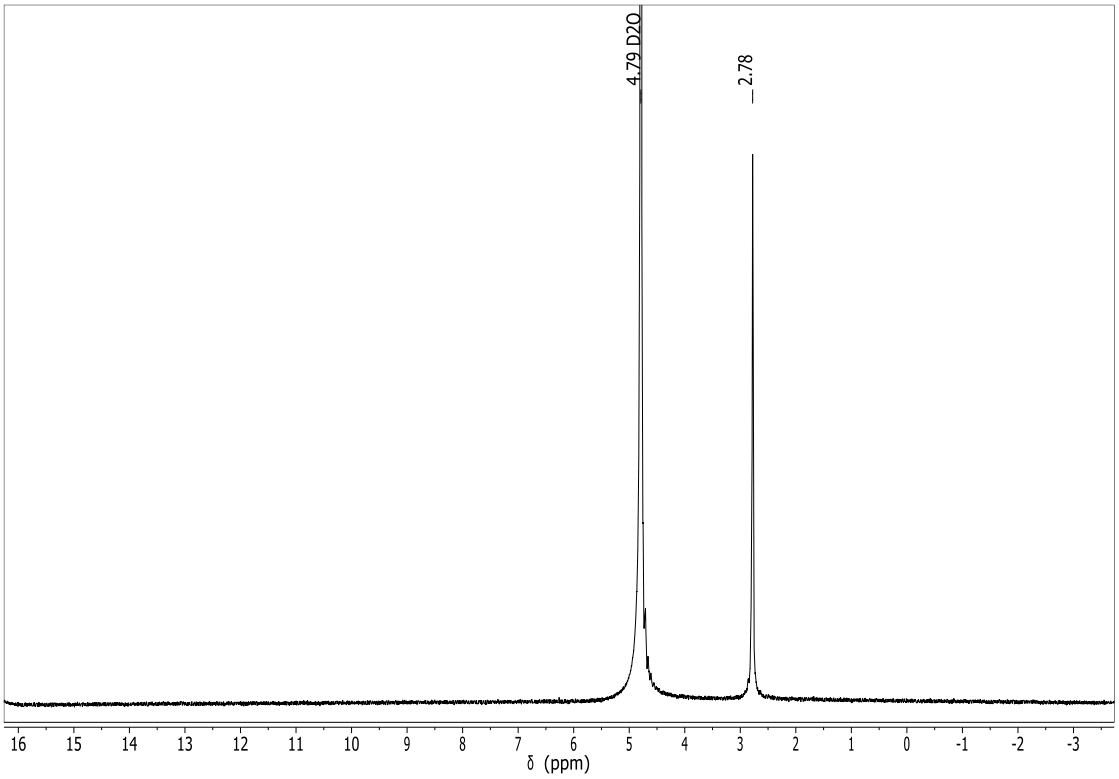

Figure S6. ^{1}H NMR spectrum of $\mathbf{2^{Cs}}$ in D_2O.

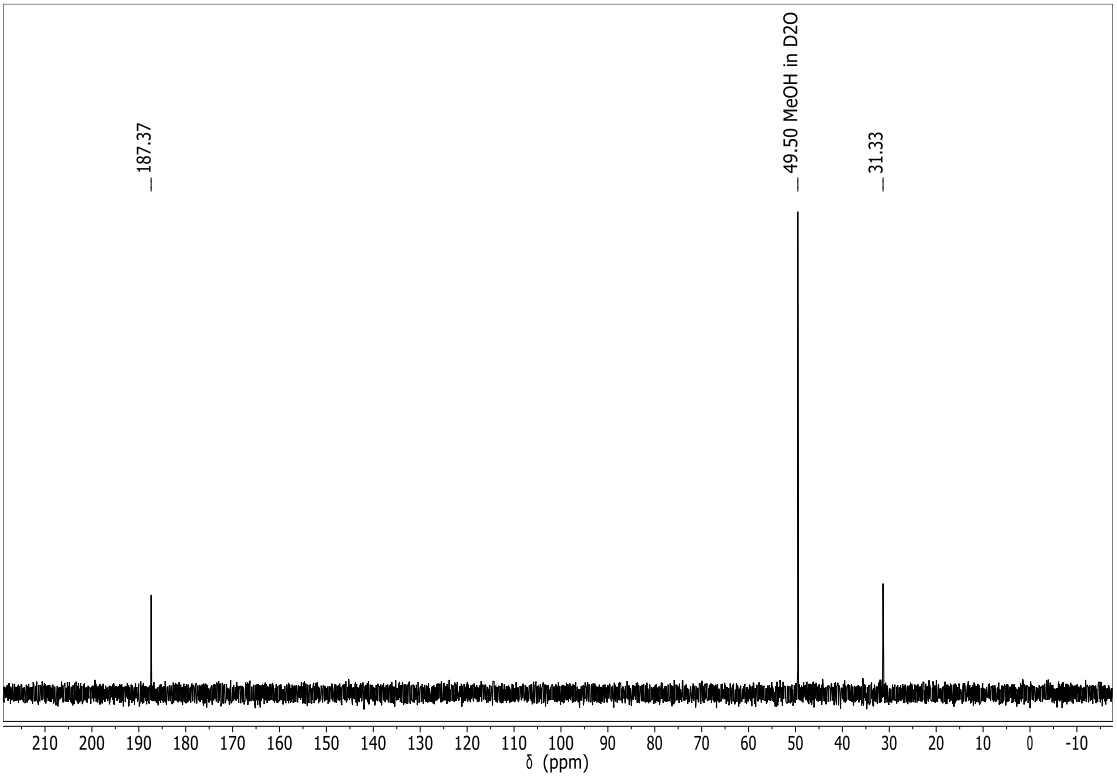

Figure S7. $^{13}C\{^{1}H\}$ NMR spectrum of $\mathbf{2^{Cs}}$ in D_2O.

5.2: NMR Spectral Data for $[(H_2O)Na]_2[Pd(succ)_4]$ (3^{Na})

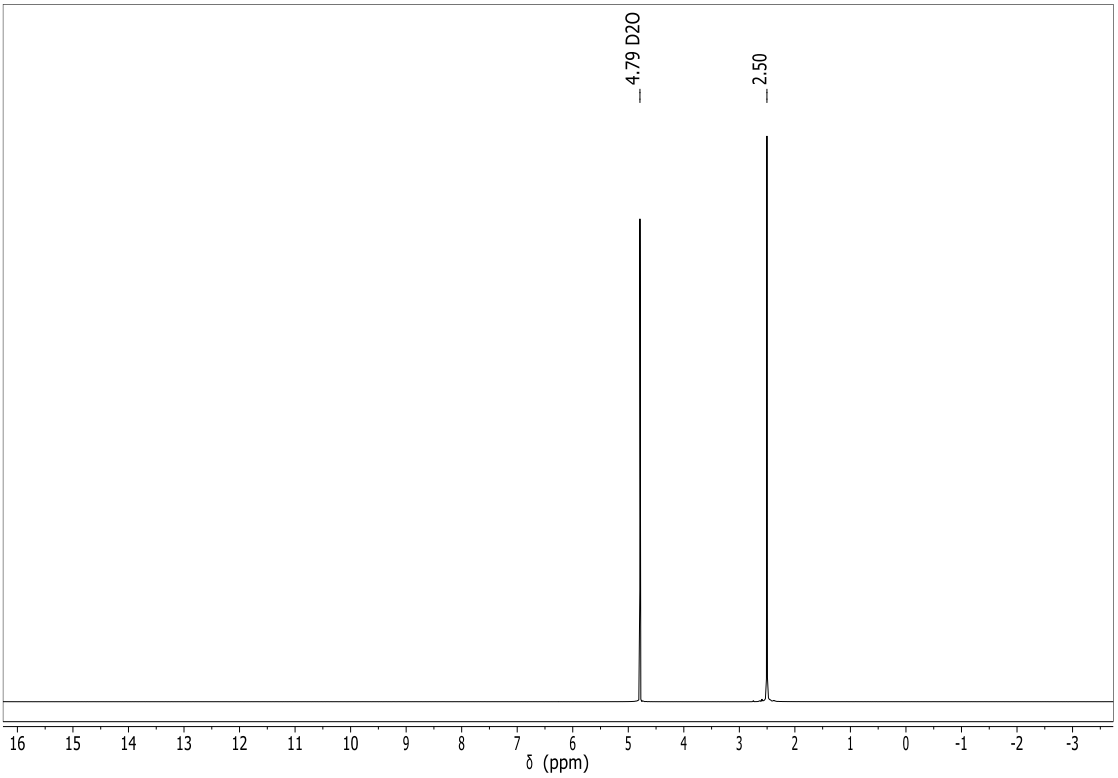

Figure S8. ^{1}H NMR spectrum of $\mathbf{3^{Na}}$ in D_2O.

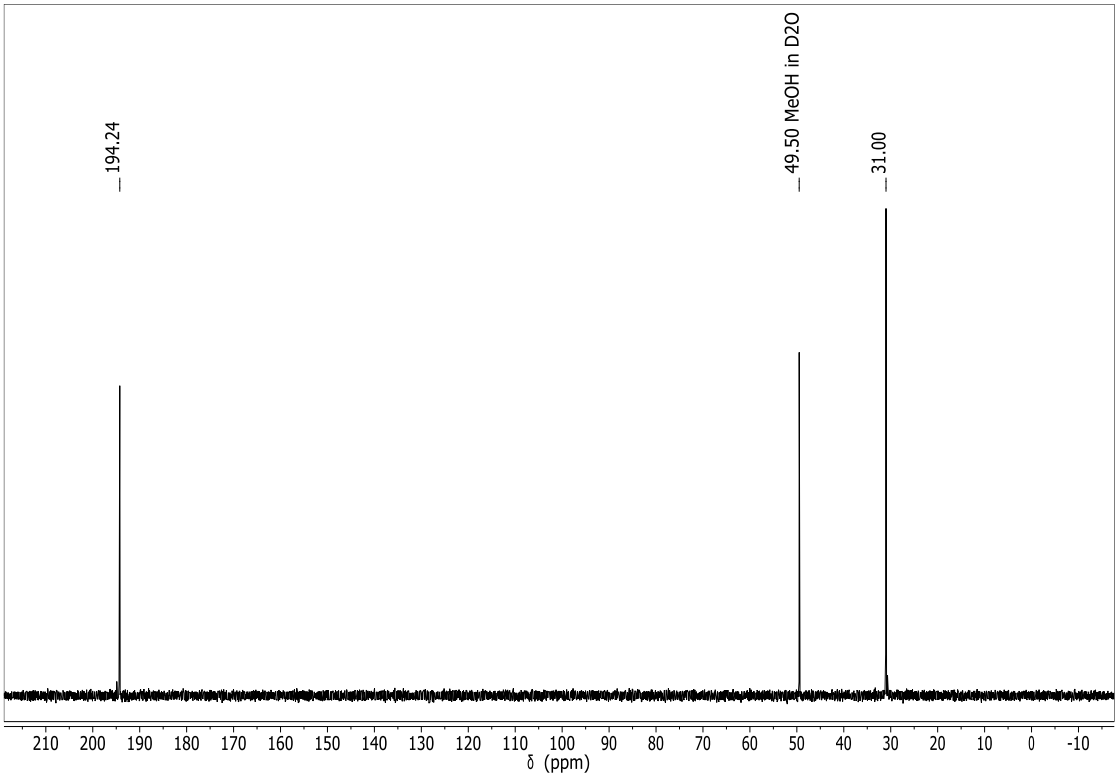

Figure S9. $^{13}C\{^{1}H\}$ NMR spectrum of $\mathbf{3^{Na}}$ in D_2O.

6: UV-vis Spectroscopy

6.1: UV-vis Spectral Data for $Cs[Ag(succ)_4] \cdot 4\ H_2O$ (2^{Cs})

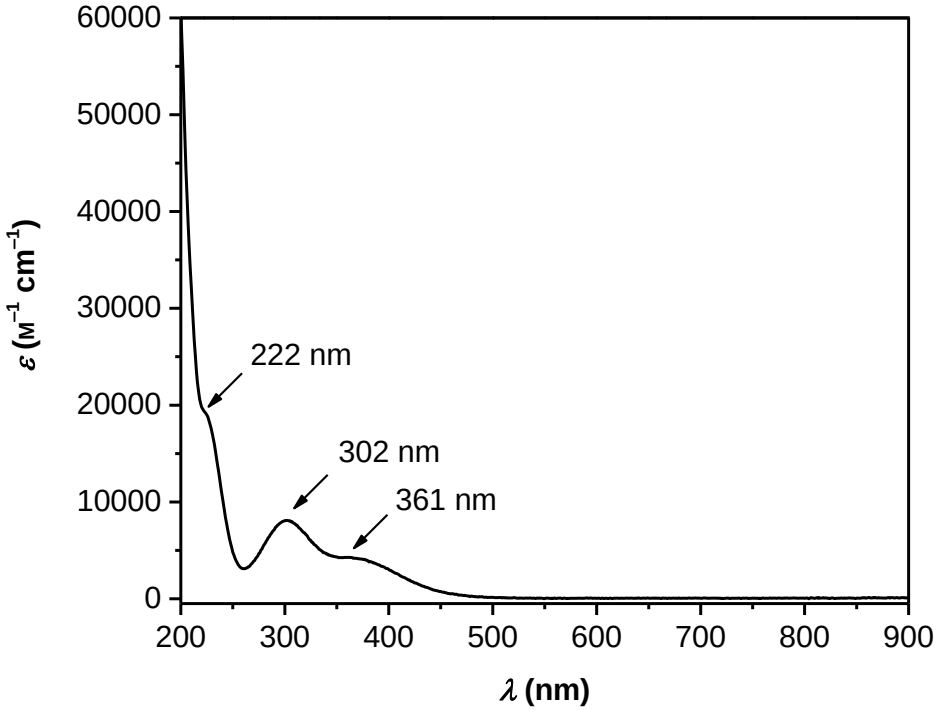

Figure S10. UV-vis spectrum of $4.7 \cdot 10^{-6}$ м $\mathbf{2^{Cs}}$ in H_2O.

6.2: UV-vis Spectral Data for $[(H_2O)Ag][Ag(succ)_4] \cdot 4\ H_2O$ (2^{Ag})

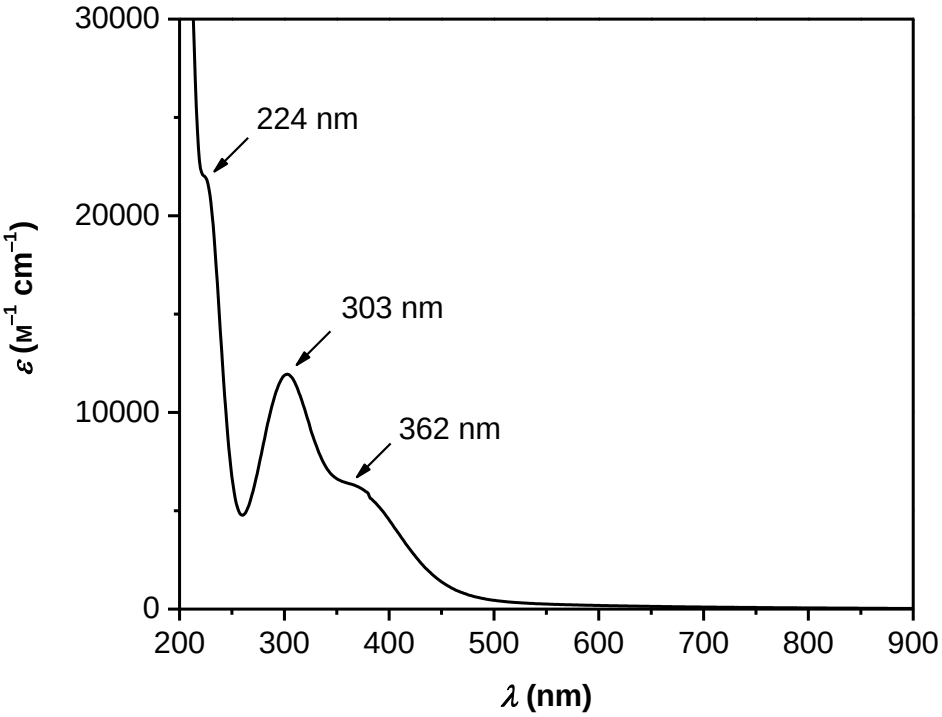

Figure S11. UV-vis spectrum of $8.3 \cdot 10^{-5}$ м $\mathbf{2^{Ag}}$ in H_2O.

6.3: UV-vis Spectral Data for 2^{Cs} and 2^{Ag} in H_2O (Overlay)

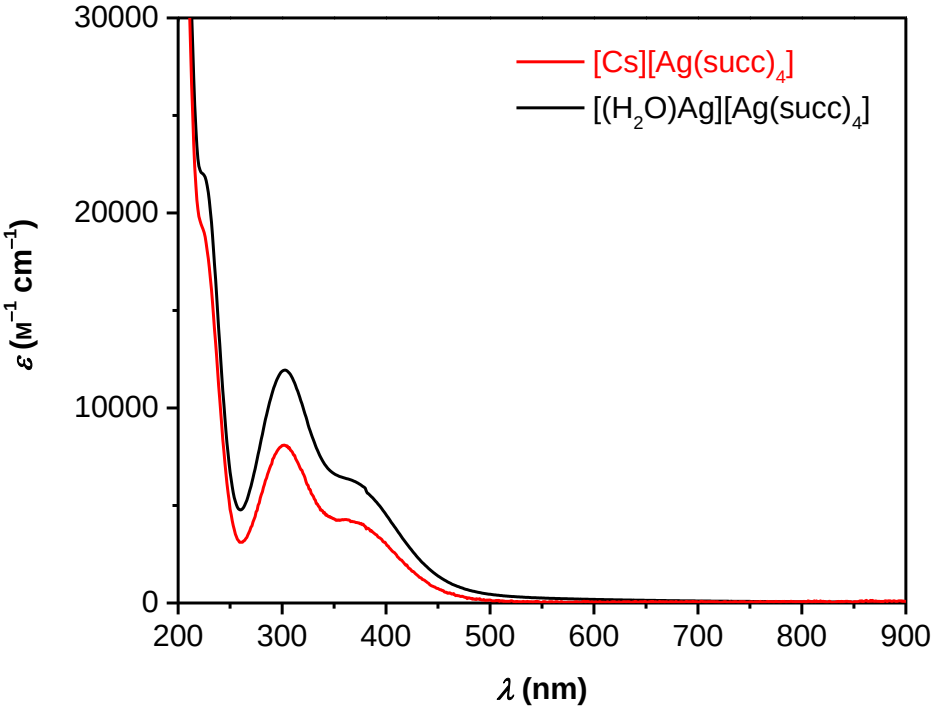

Figure S12. Overlay of UV-vis spectra of $\mathbf{2^{Cs}}$ and $\mathbf{2^{Ag}}$ in H_2O.

6.4: UV-vis Spectral Data for 2^{Cs} and 2^{Ag} in solid KBr (Overlay)

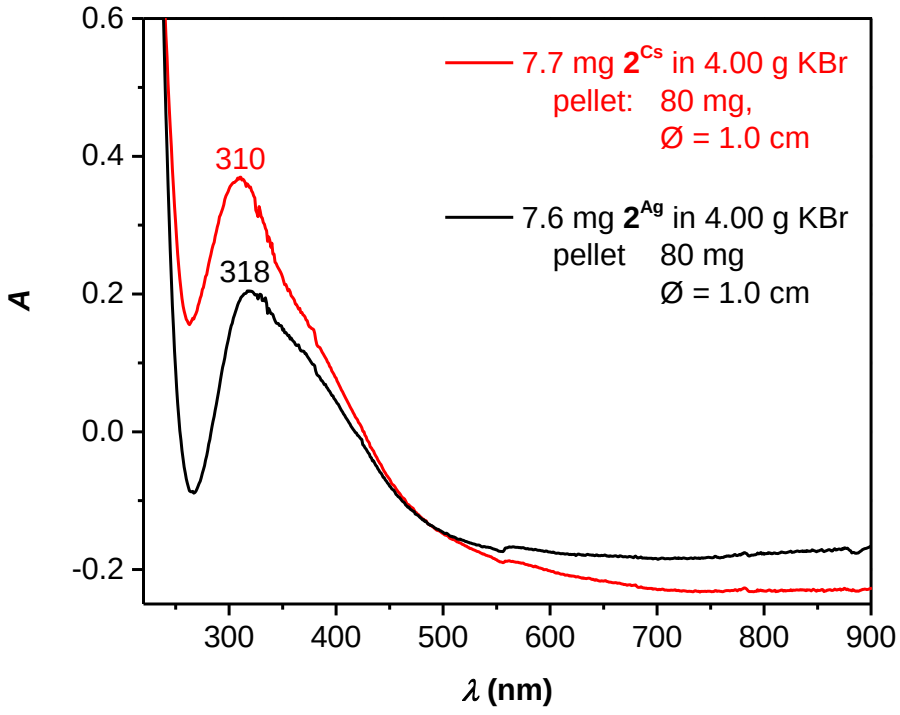

Figure S13. Overlay of UV-vis spectra of $\mathbf{2^{Cs}}$ and $\mathbf{2^{Ag}}$ in solid KBr.

6.5: UV-vis Spectral Data for $[(H_2O)Na]_2[Pd(succ)_4]$ (3^{Na})

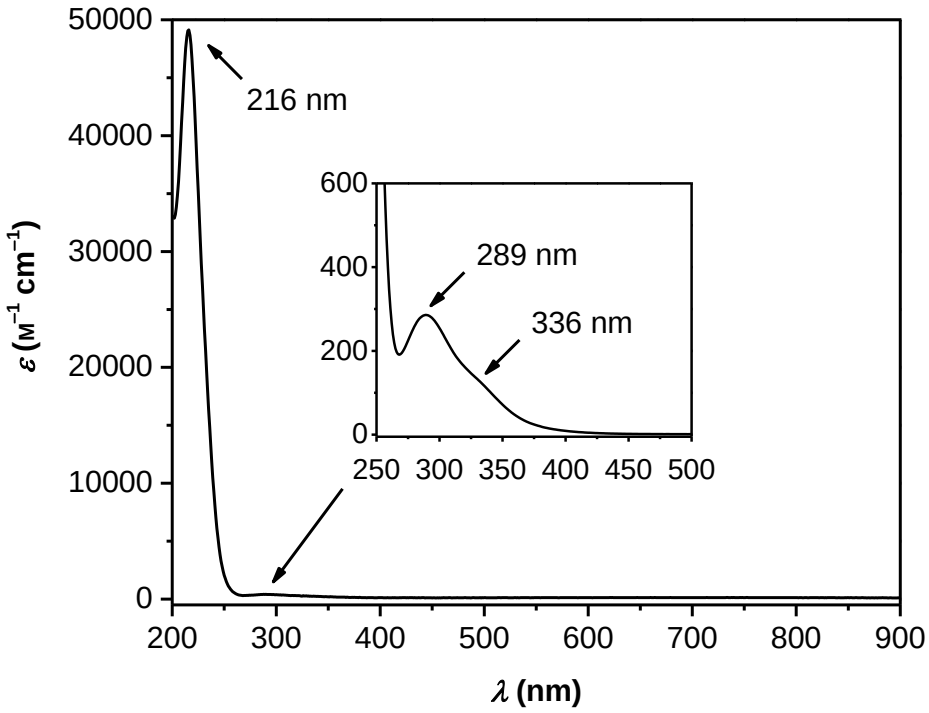

Figure S14. UV-vis spectrum of $1.8 \cdot 10^{-5}$ м **3^{Na}** in H_2O; inset: $3.5 \cdot 10^{-3}$ м.

6.6: UV-vis Spectral Data for Na(succ)

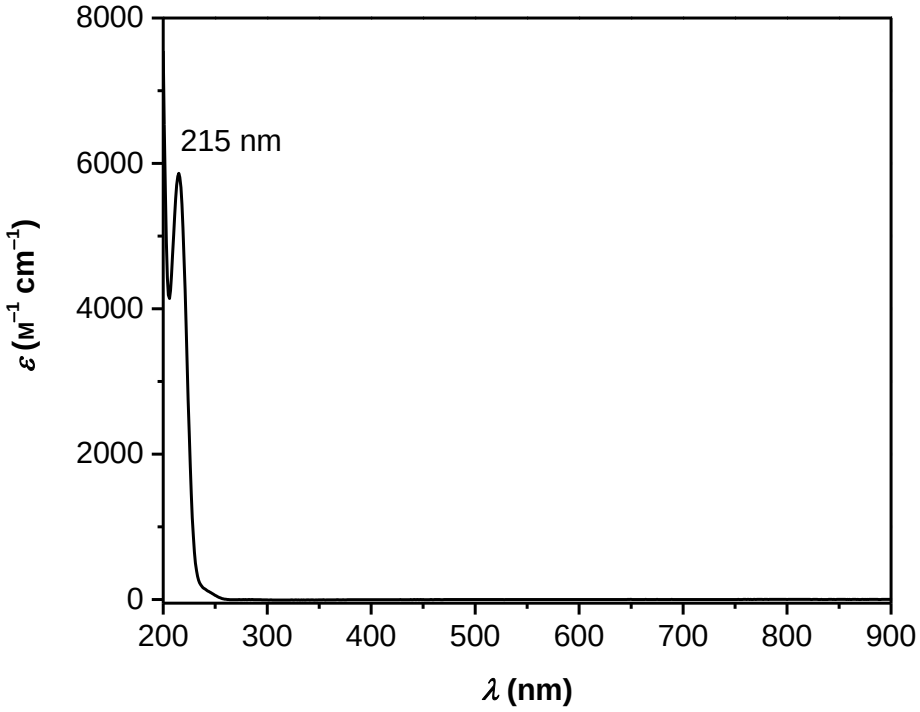

Figure S15. UV-vis spectrum of $2.5 \cdot 10^{-4}$ м Na(succ) in H_2O.

7: Kinetic Studies of Decomposition of 2^{Cs} in Aqueous Solution

Decomposition of 2^{Cs} in neutral solution was monitored by dissolving $\mathbf{2^{Cs}}$ (3.3 mg, 4.7 µmol) in water (38.5 ml, 120 µM) and transferring the solution to a quartz cuvette background corrected with the solvent. 150 s after dissolution, 50 consecutive UV-vis spectra were recorded at 300 s intervals.

Decomposition of 2^{Cs} in basic solution was monitored by dissolving $\mathbf{2^{Cs}}$ (2.2 mg, 3.1 µmol) in aqueous NaOH (pH = 12.73, 17.2 ml, 180 µM) and transferring the solution to a quartz cuvette background corrected with the solvent. 120 s after dissolution, 20 consecutive UV-vis spectra were recorded at 120 s intervals.

Decomposition of 2^{Cs} in acidic solution was monitored by dissolving $\mathbf{2^{Cs}}$ (5.0 mg, 7.1 µmol) in aqueous $HClO_4$ (pH = 3.01, 29.3 ml, 240 µM) and transferring the solution to a quartz cuvette background corrected with the solvent. 120 s after dissolution, 6 consecutive UV-vis spectra were recorded at 120 s intervals.

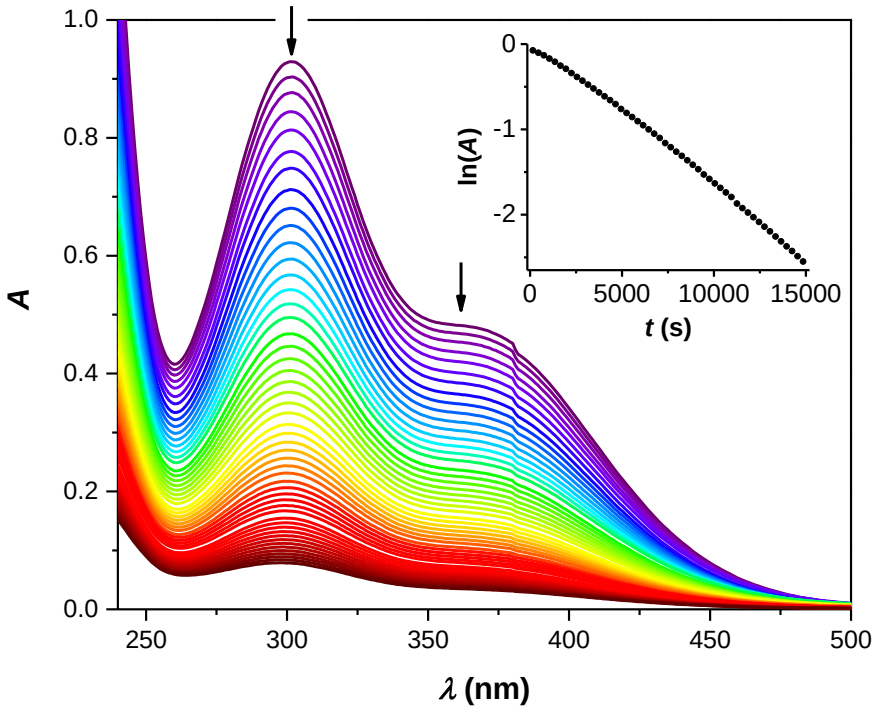

Figure S16. UV-vis spectra showing the decomposition of $\mathbf{2^{Cs}}$ in neutral solution (demineralized water, pH = 6.50). Inset: time-dependence of ln(*A*) at λ_{max} = 302 nm, $t_{½}$ = 68 minutes.

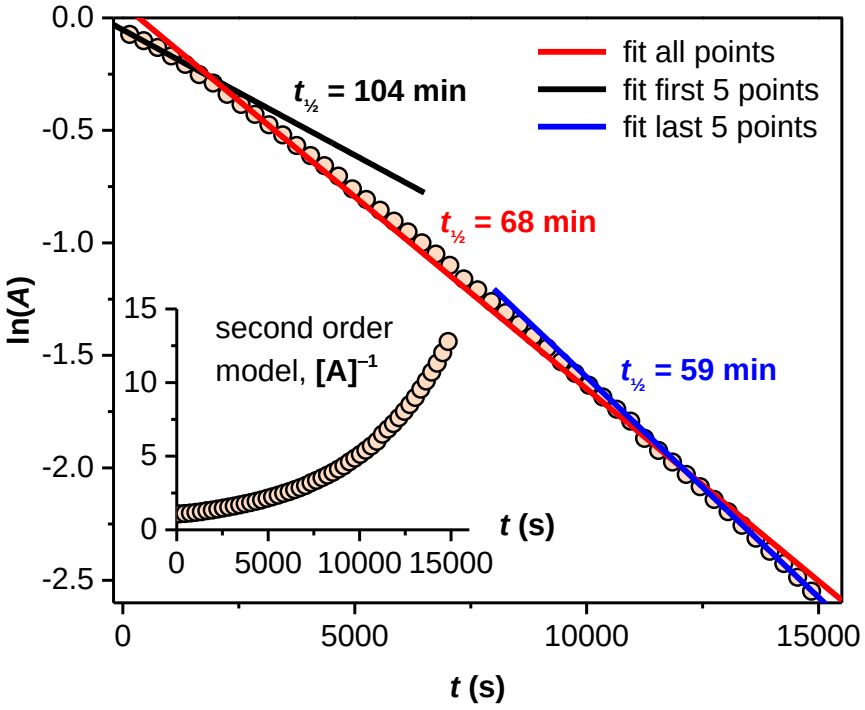

Figure S17. Linear fits (all points, first 5 points, last 5 points) to ln(*A*) *versus* time for the decomposition of **2**^{Cs} in neutral solution (demineralized water, pH = 6.50). Inset: Plot of A^{-1} *versus* time, showing how the decomposition deviates from second order kinetics.

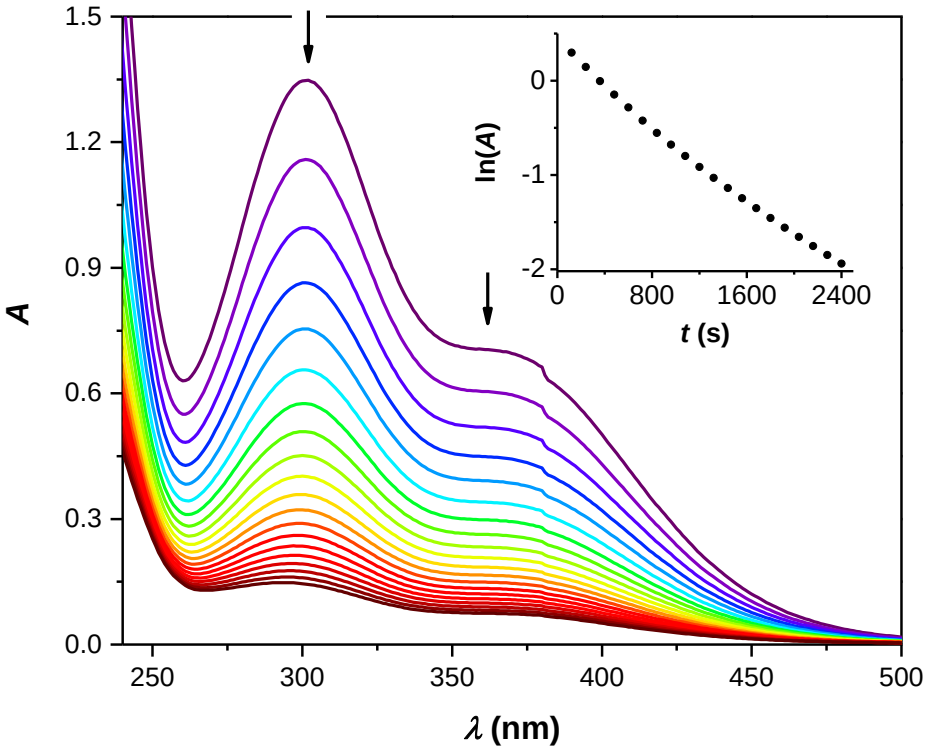

Figure S18. UV-vis spectra showing the decomposition of **2**^{Cs} in basic solution (aq. NaOH, pH = 12.73). Inset: time-dependence of ln(*A*) at λ_{max} = 302 nm, $t_{½}$ = 12 minutes.

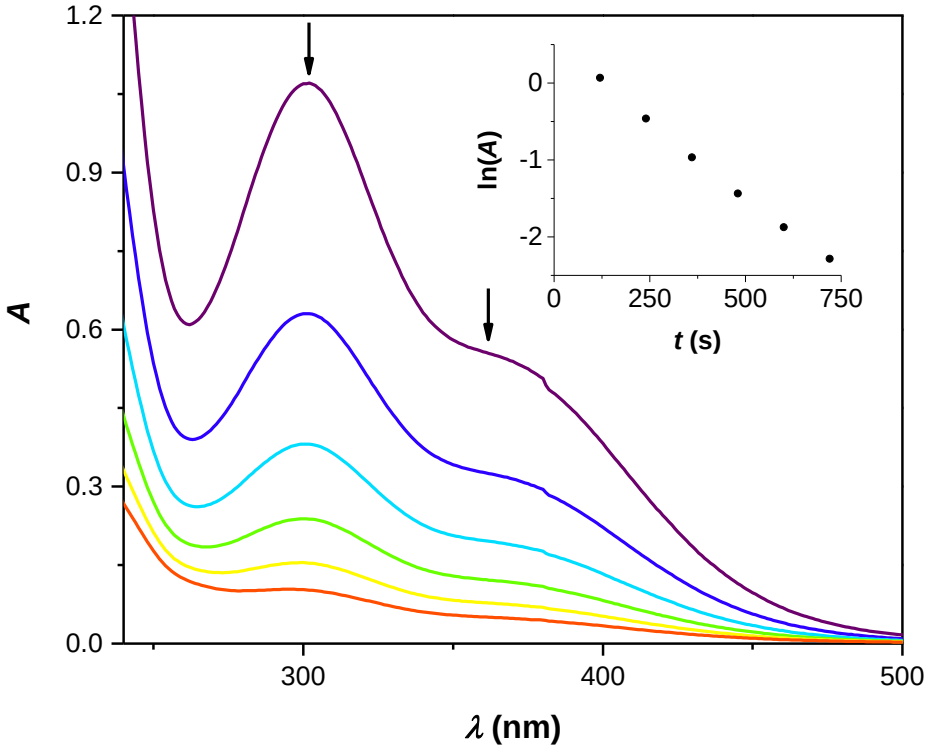

Figure S19. UV-vis spectra showing the decomposition of **2**^{Cs} in acidic solution (aq. $HClO_4$, pH = 3.01). Inset: time-dependence of ln(*A*) at λ_{max} = 302 nm, $t_{½}$ = 180 s.

8: Mass Spectrometry

8.1: Mass Spectrometric Data for $Cs[Ag(succ)_4] \cdot 4\ H_2O$ (2^{Cs})

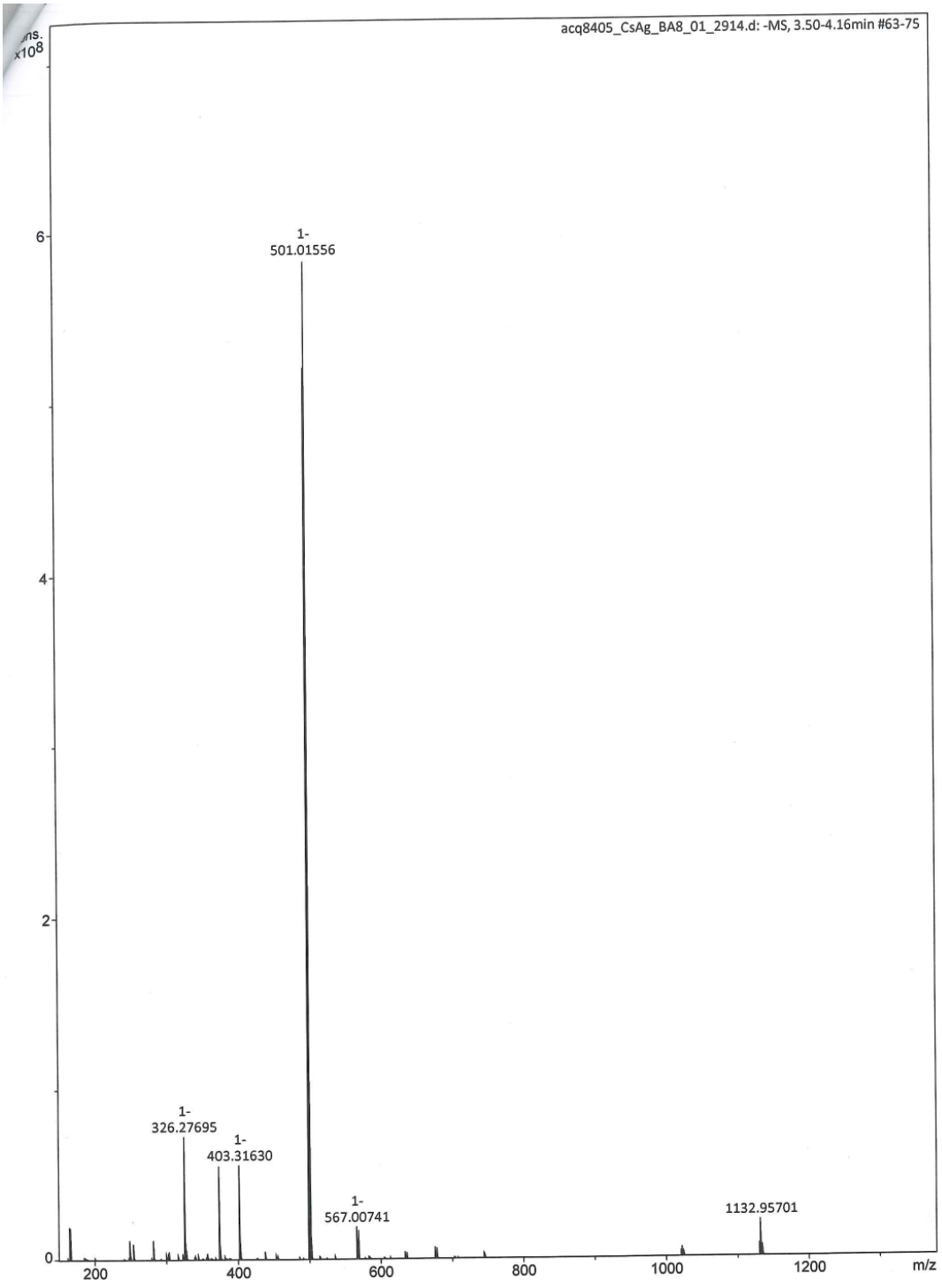

Figure S20. Negative mode ESI-MS spectrum of $\mathbf{2^{Cs}}$.

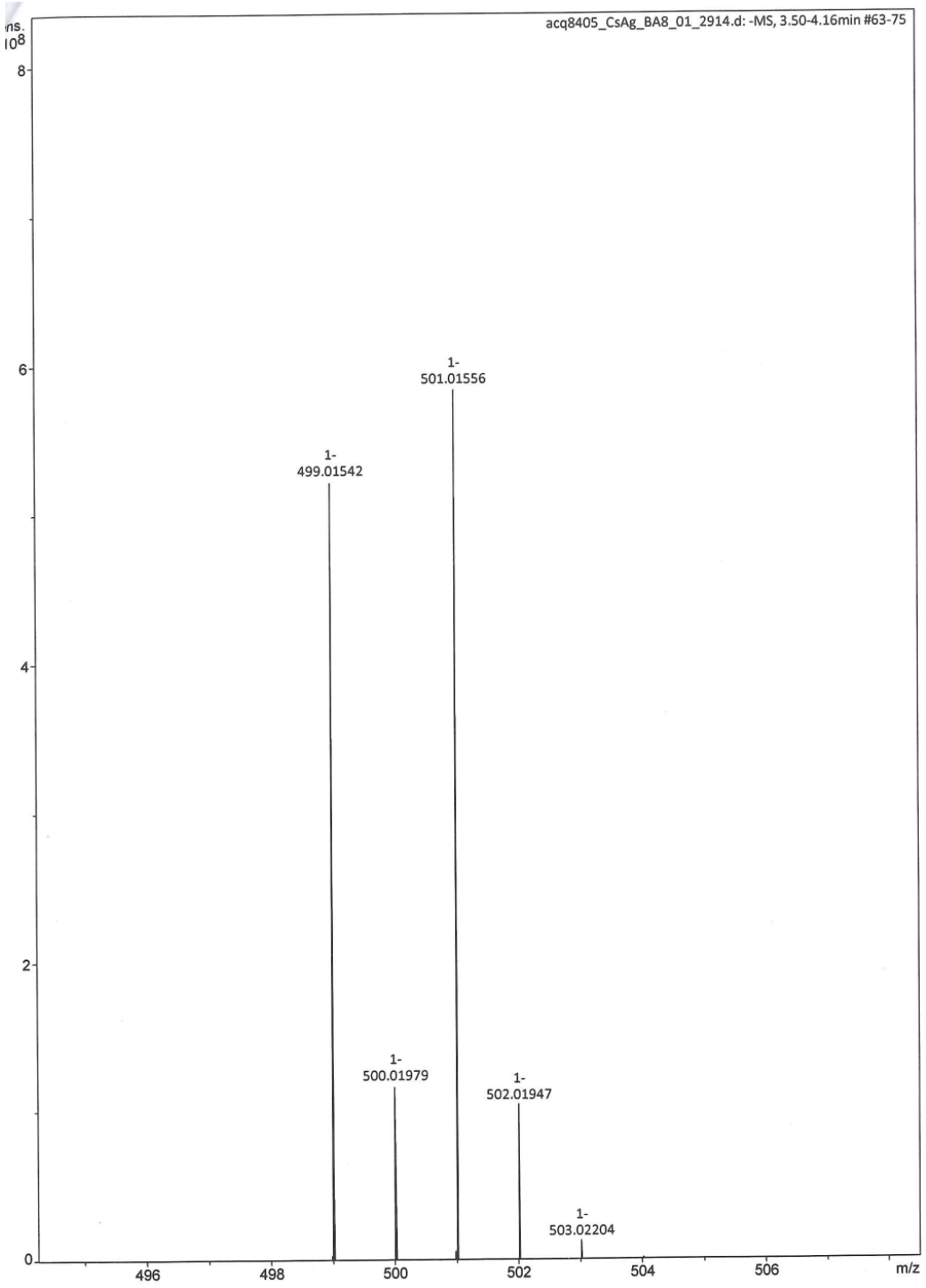

Figure S21. Negative mode ESI-MS spectrum of $\mathbf{2}^{\mathbf{Cs}}$, $[Ag(succ)_4]^-$, calculated: *m*/*z* = 499.00 (100.0%), 501.00 (96.3%), 500.00 (19.2%), 502.00 (18.3%), 503.01 (3.2%).

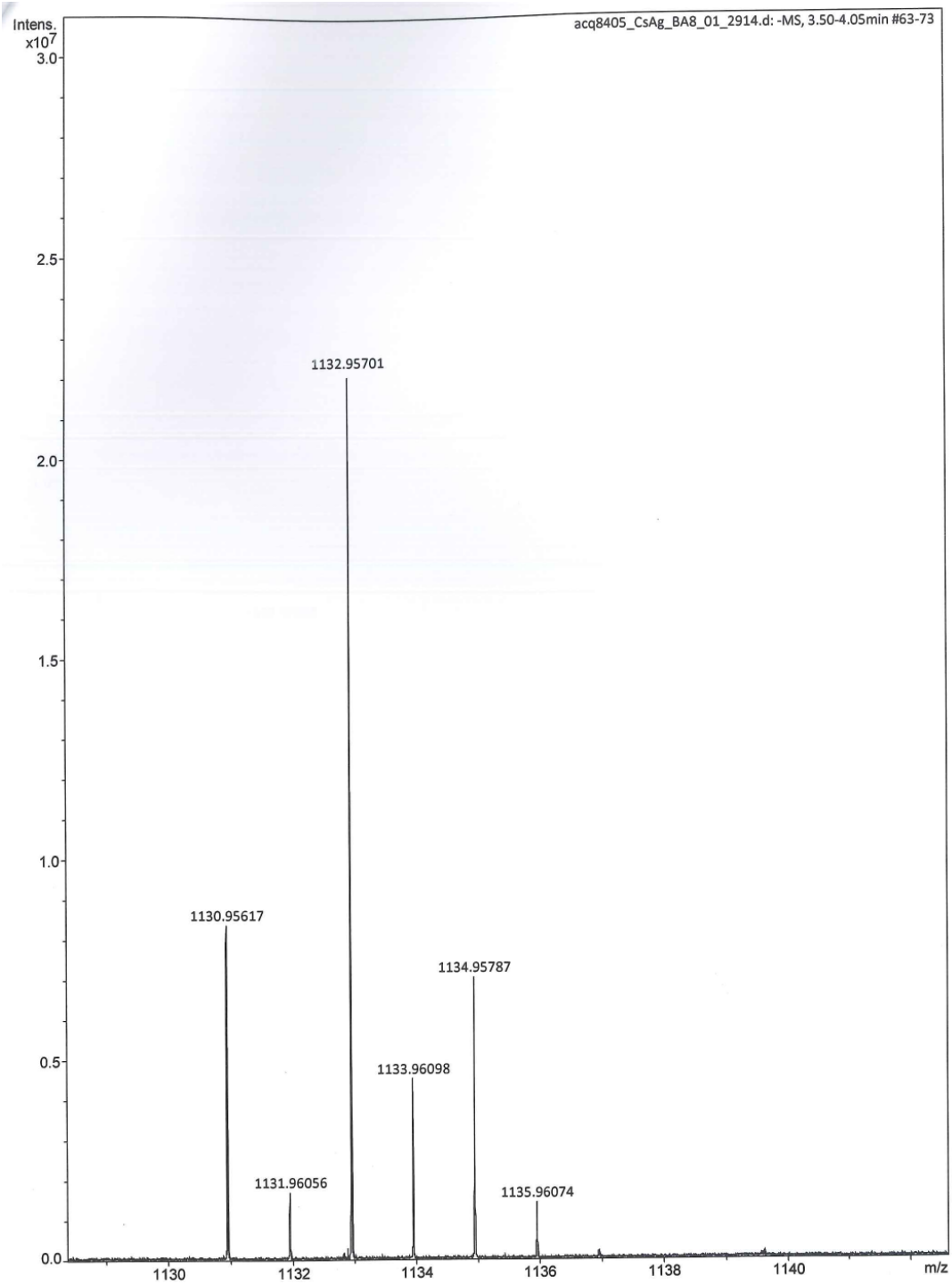

Figure S22. Negative mode ESI-MS spectrum of **2^{Cs}**, $[Cs\{Ag(succ)_4\}_2]^-$, calculated: *m*/*z* = 1132.91 (100.0%), 1134.91 (54.1%), 1130.91 (50.9%), 1133.91 (37.5%), 1131.91 (19.6%), 1135.91 (19.0%), 1136.91 (5.0%).

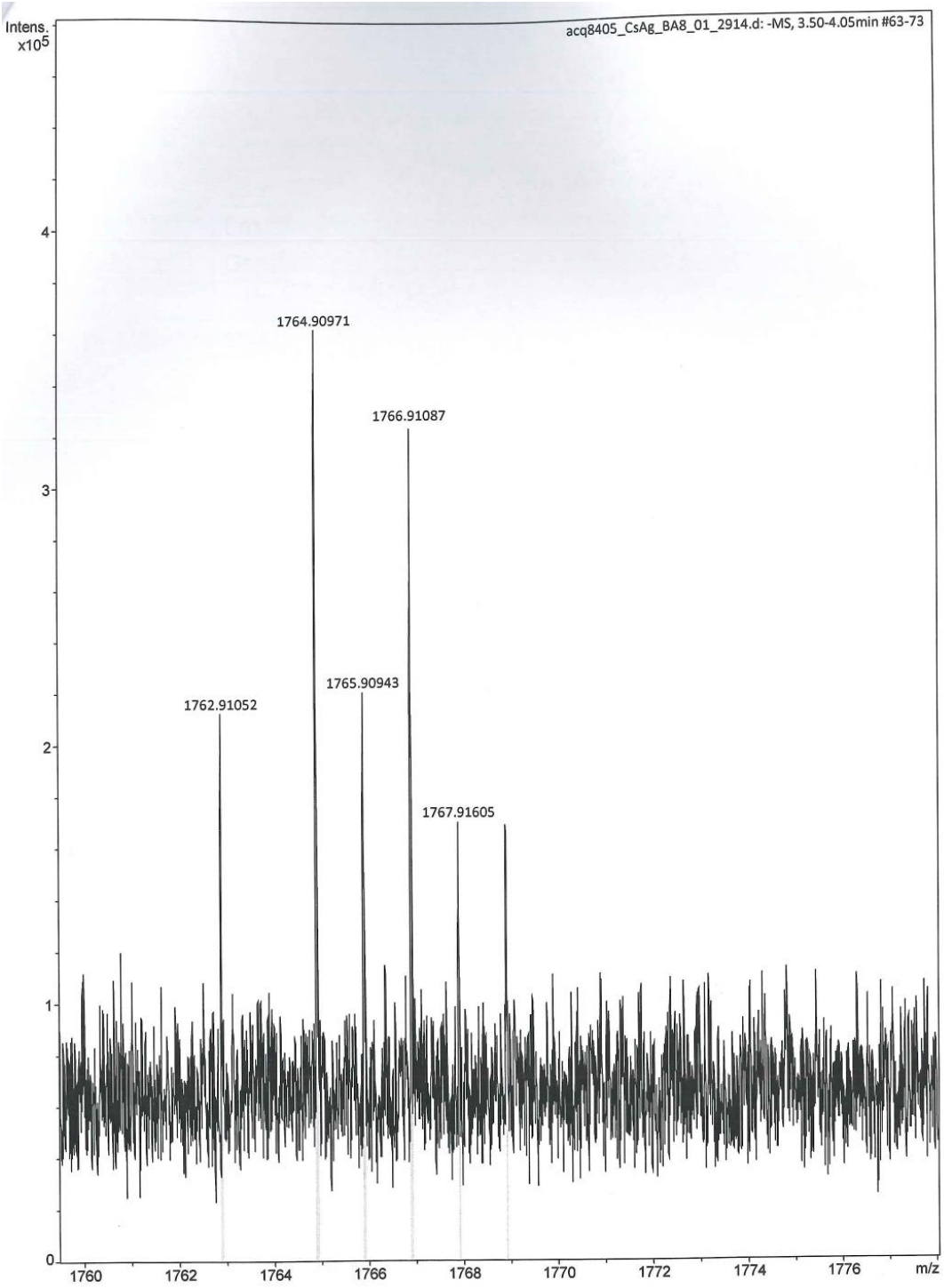

Figure S23. Negative mode ESI-MS spectrum of $\mathbf{2^{Cs}}$, $[Cs_2\{Ag(succ)_4\}_3]^-$, calculated: *m*/*z* = 1766.82 (100.0%), 1764.82 (93.8%), 1765.82 (52.2%), 1767.82 (52.0%), 1768.82 (43.5%), 1762.82 (31.3%).

8.2: Mass Spectrometric Data for $[(H_2O)Na]_2[Pd(succ)_4]$ (3^{Na})

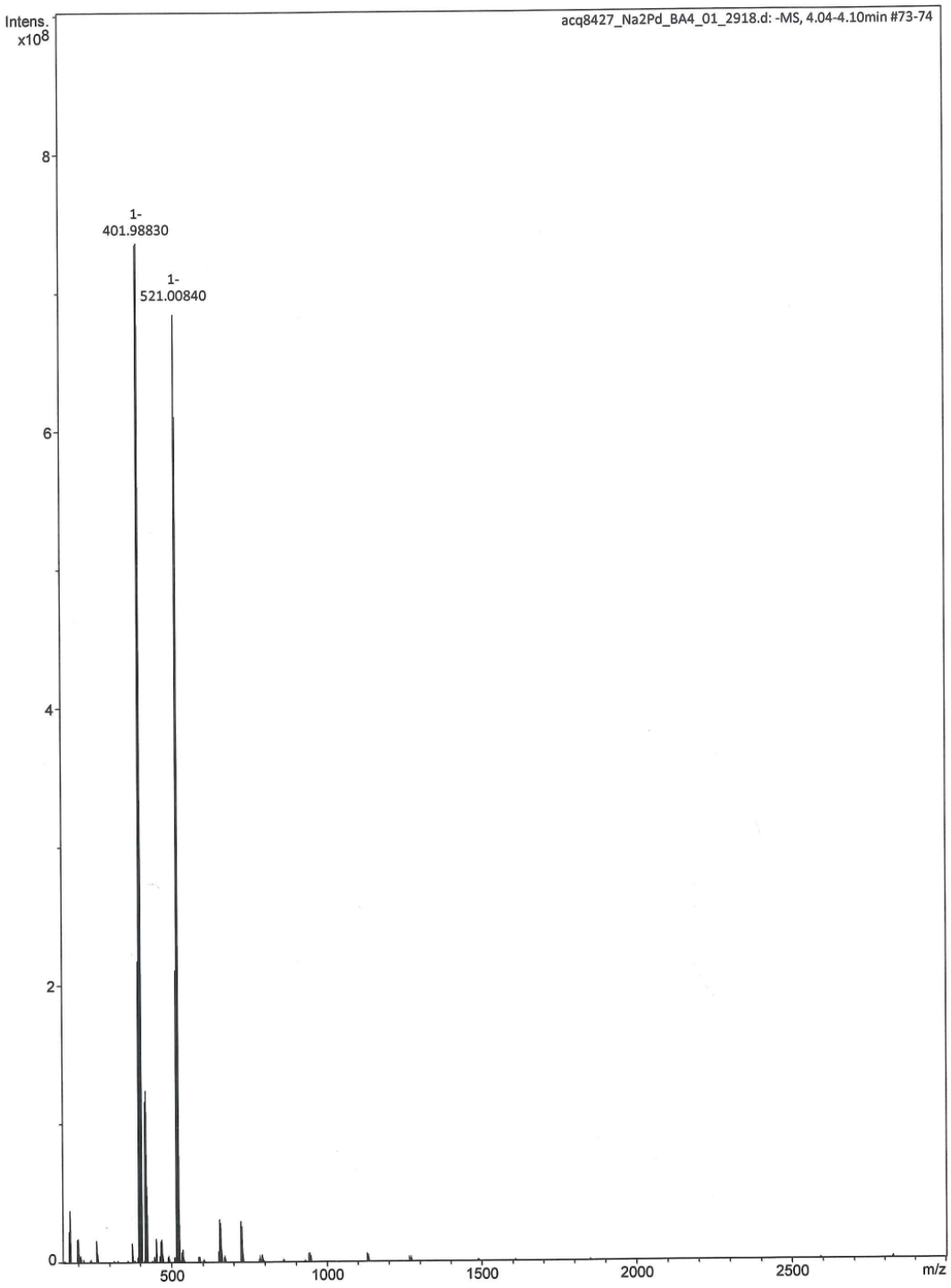

Figure S24. Negative mode ESI-MS spectrum of $\mathbf{3^{Na}}$.

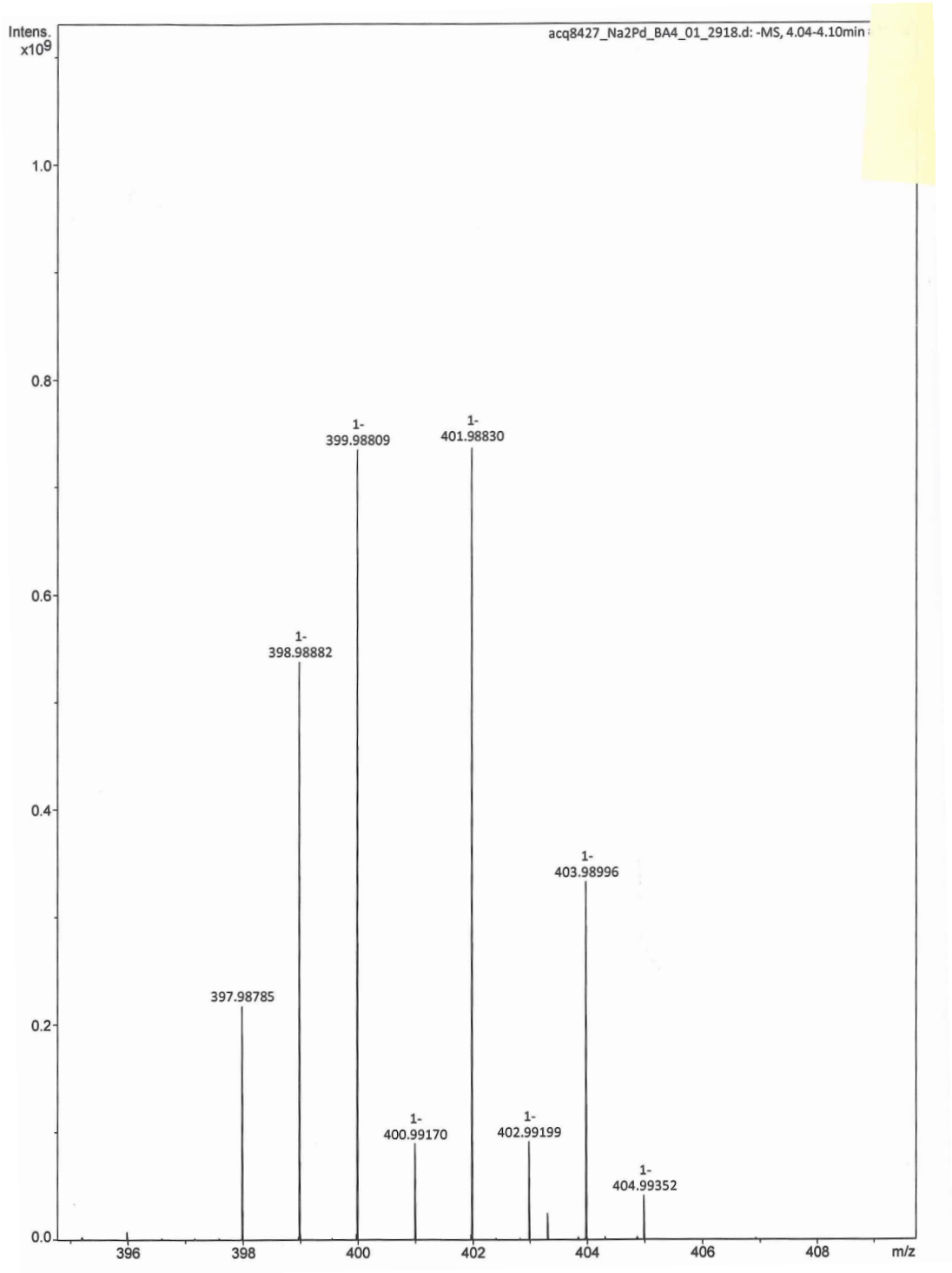

Figure S25. Negative mode ESI-MS spectrum of $\mathbf{3^{Na}}$, $[Pd(succ)_3]^-$, calculated: *m*/*z* = 399.98 (100.0%), 401.98 (88.0%), 398.98 (77.8%), 403.98 (40.0%), 397.98 (36.2%), 400.98 (14.5%), 402.98 (12.6%), 404.98 (5.7%), 395.98 (3.3%).

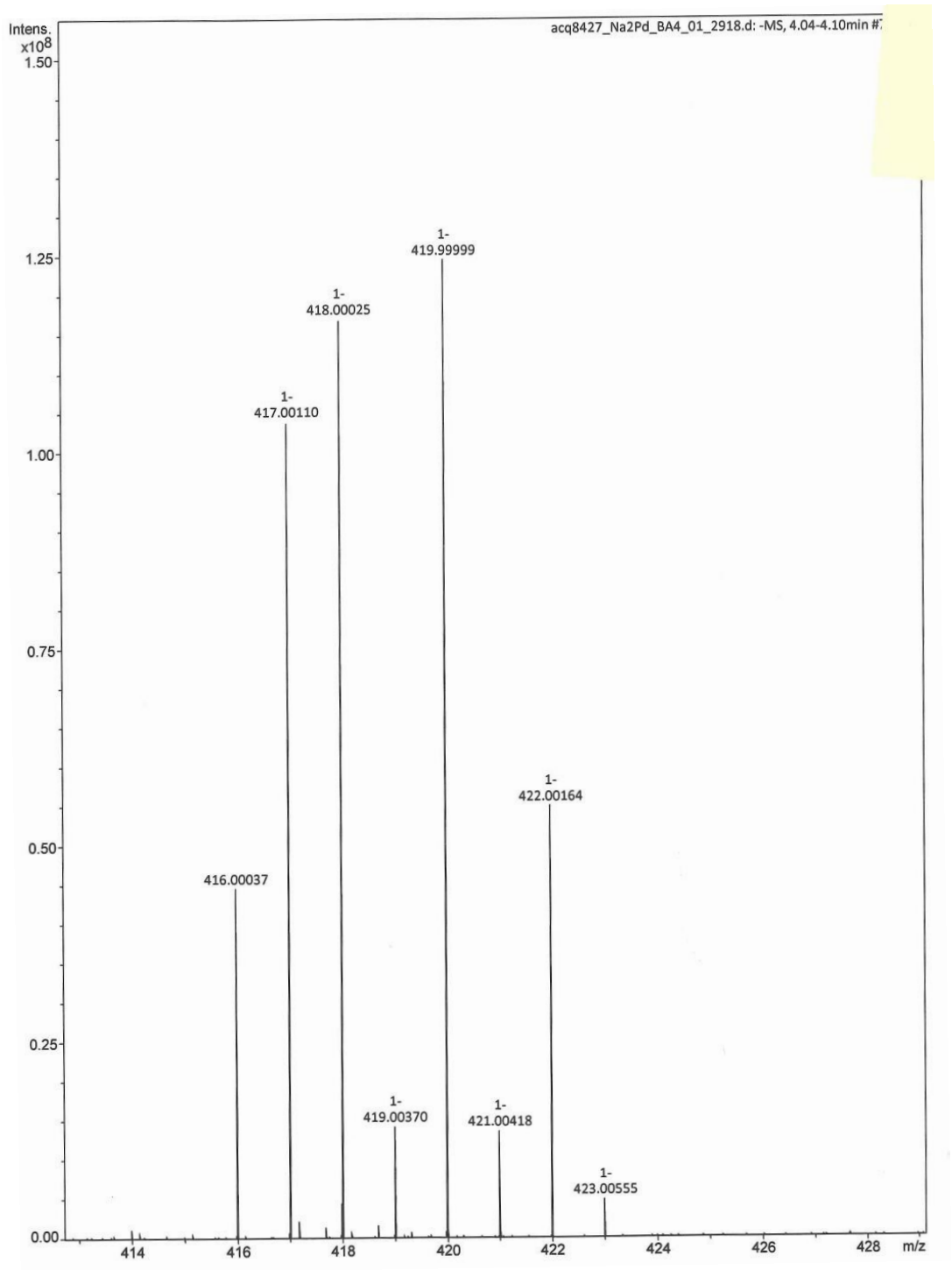

Figure S26. Negative mode ESI-MS spectrum of $\mathbf{3^{Na}}$, $[Pd(succ)_3(H_2O)]^-$, calculated: *m*/*z* = 417.99 (100.0%), 419.99 (88.1%), 416.99 (77.7%), 421.99 (40.1%), 415.99 (36.2%), 418.99 (14.7%), 420.99 (12.7%), 422.99 (5.7%), 413.99 (3.3%).

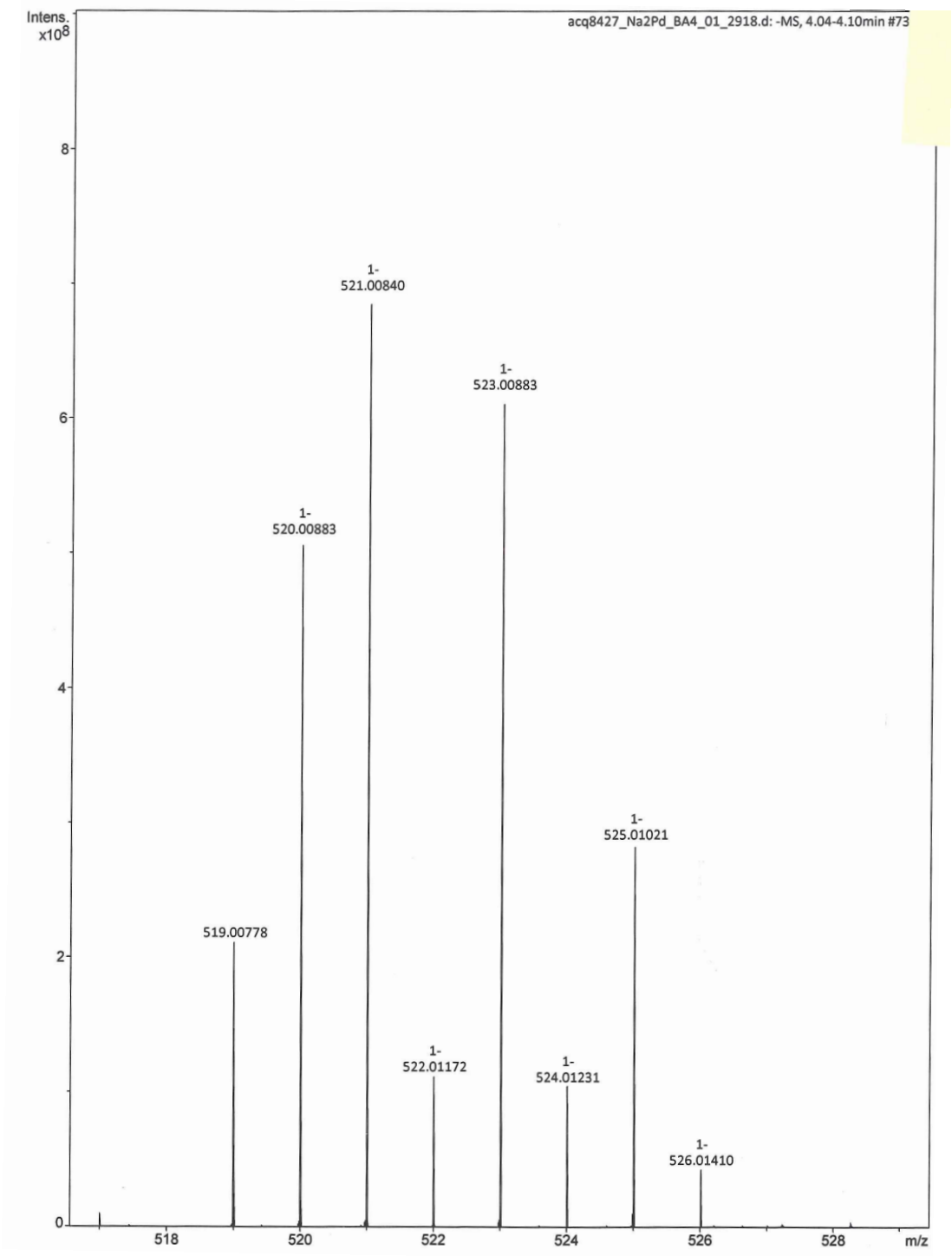

Figure S27. Negative mode ESI-MS spectrum of $\mathbf{3}^{\mathbf{Na}}$, $[Na\{Pd(succ)_4\}]^-$, calculated: *m*/*z* = 520.99 (100.0%), 522.99 (85.9%), 519.99 (76.5%), 524.99 (39.5%), 518.99 (34.9%), 521.99 (19.0%), 523.99 (16.3%), 525.99 (7.4%), 516.99 (3.2%), 527.00 (1.3%).

9: Single Crystal X-ray Diffraction

9.1 Crystallographic Tables

Table S1. Crystallographic data for $\mathbf{2^{Cs}}$ and $\mathbf{2^{Rb}}$.

Complex	$\mathbf{2^{Cs}}$	$\mathbf{2^{Rb}}$
CCDC entry	2365919	2365920
Empirical formula	$C_{16}H_{24}AgCsN_4O_{12}$	$C_{16}H_{24}AgN_4O_{12}Rb$
Formula weight	705.17	657.73
T / K	122(2)	100(2)
Crystal system	tetragonal	tetragonal
Space group	*I*4/*m*	*I*4/*m*
a / Å	11.3504(5)	11.3963(9)
b / Å	11.3504(5)	11.3963(9)
c / Å	8.7443(4)	8.5069(6)
α / °	90	90
β / °	90	90
γ / °	90	90
V / Å^3	1126.54(11)	1104.84(19)
Z	2	2
ρ_{calc} / g cm^{-3}	2.079	1.977
μ / mm^{-1}	2.558	3.173
2θ range / °	5.076 – 56.554	5.054 – 60.96
Reflections collected	6759	10557
Independent reflections	748 [R_{int} = 0.0203]	896 [R_{int} = 0.0571]
Data / restraints / parameters	748 / 0 / 47	896 / 0 / 48
Goodness-of-fit on F^2	1.133	1.125
Final R indexes [$I \geq 2\sigma(I)$]	R_1 = 0.0218, wR_2 = 0.0511	R_1 = 0.0214, wR_2 = 0.0438
Final R indexes [all data]	R_1 = 0.0230, wR_2 = 0.0518	R_1 = 0.0305, wR_2 = 0.0459
Largest diff. peak/hole / e Å^{-3}	2.40 / –0.96	0.45 / –0.81

Table S2. Crystallographic data for $\mathbf{2^K}$ and $\mathbf{2^{Ag}}$.

Complex	$\mathbf{2^K}$	$\mathbf{2^{Ag}}$
CCDC entry	2365917	2365916
Empirical formula	$C_{16}H_{24}AgKN_4O_{12}$	$C_{16}H_{26}Ag_2N_4O_{13}$
Formula weight	611.35	698.15
T / K	100(2)	293.15
Crystal system	tetragonal	tetragonal
Space group	$I4/m$	$I4/m$
a / Å	11.554(2)	11.321(3)
b / Å	11.554(2)	11.321(3)
c / Å	8.420(3)	9.154(3)
α / °	90	90
β / °	90	90
γ / °	90	90
V / Å^3	1124.1(8)	1173.2(8)
Z	2	2
ρ_{calc} / g cm^{-3}	1.806	1.976
μ / mm^{-1}	1.153	1.742
2θ range / °	4.986 – 62.01	5.088 – 59.09
Reflections collected	11071	3315
Independent reflections	961 [R_{int} = 0.0291]	876 [R_{int} = 0.0228]
Data / restraints / parameters	961 / 0 / 48	876 / 2 / 54
Goodness-of-fit on F^2	1.209	1.149
Final R indexes [$I \geq 2\sigma(I)$]	R_1 = 0.0143, wR_2 = 0.0395	R_1 = 0.0293, wR_2 = 0.0811
Final R indexes [all data]	R_1 = 0.0143, wR_2 = 0.0395	R_1 = 0.0299, wR_2 = 0.0817
Largest diff. peak/hole / e Å^{-3}	0.31 / –0.47	0.44 / –1.55

Table S3. Crystallographic data for $\mathbf{3^{Na}}$ and $Cs[Ag(succ)_2] \cdot 4\ H_2O$ ($\mathbf{1^{Cs}}$).

Complex	$\mathbf{3^{Na}}$	$Cs[Ag(succ)_2] \cdot 4\ H_2O$ ($\mathbf{1^{Cs}}$)
CCDC entry	2365918	2372376
Empirical formula	$C_{16}H_{24}N_4Na_2O_{12}Pd$	$C_8H_{16}AgCsN_2O_8$
Formula weight	616.77	509.01
T / K	122(2)	120(2)
Crystal system	triclinic	triclinic
Space group	P–1	P–1
a / Å	8.2595(5)	9.7035(6)
b / Å	9.1546(6)	13.0999(8)
c / Å	9.1795(6)	13.5608(9)
α / °	64.956(2)	68.125(2)
β / °	67.171(2)	73.051(2)
γ / °	87.677(2)	76.873(2)
V / Å^3	573.18(6)	1516.49(17)
Z	1	4
ρ_{calc} / g cm^{-3}	1.787	2.229
μ / mm^{-1}	0.918	3.730
2θ range / °	4.966 – 58.26	4.892 – 59.15
Reflections collected	23185	51926
Independent reflections	3084 [R_{int} = 0.0354]	8488 [R_{int} = 0.0416]
Data / restraints / parameters	3084 / 0 / 189	8488 / 1 / 412
Goodness-of-fit on F^2	1.093	1.026
Final R indexes [$I \geq 2\sigma(I)$]	R_1 = 0.0180, wR_2 = 0.0446	R_1 = 0.0218, wR_2 = 0.0419
Final R indexes [all data]	R_1 = 0.0184, wR_2 = 0.0448	R_1 = 0.0346, wR_2 = 0.0451
Largest diff. peak/hole / e Å^{-3}	0.46 / –0.91	0.71 / –0.88

9.2 Thermal Ellipsoid Plots

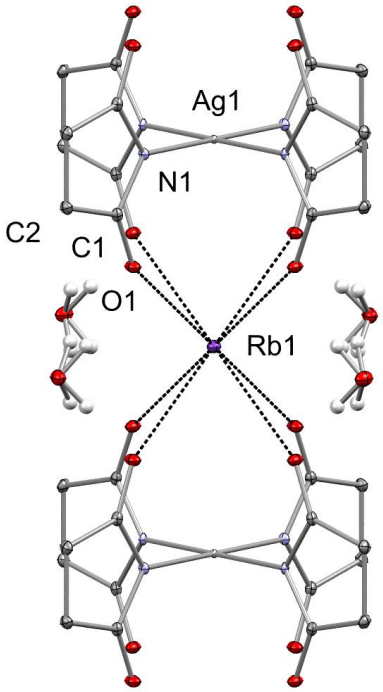

Figure S28. Thermal ellipsoid plot showing section of polymeric $\mathbf{2^{Rb}}$ at 50% probability. H atoms (except on H_2O) are omitted.

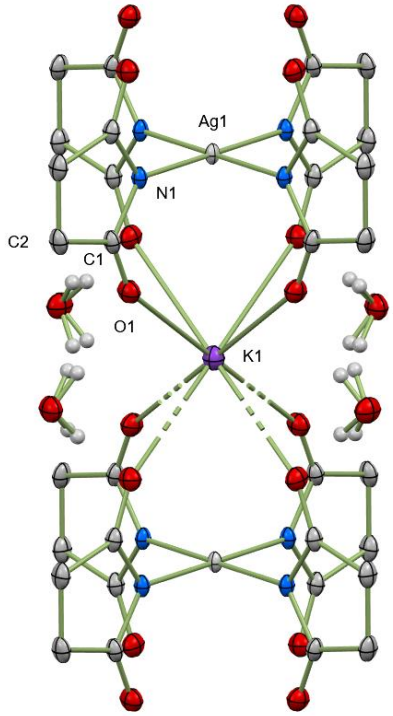

Figure S29. Thermal ellipsoid plot showing section of polymeric $\mathbf{2^{K}}$ at 50% probability. H atoms (except on H_2O) are omitted.

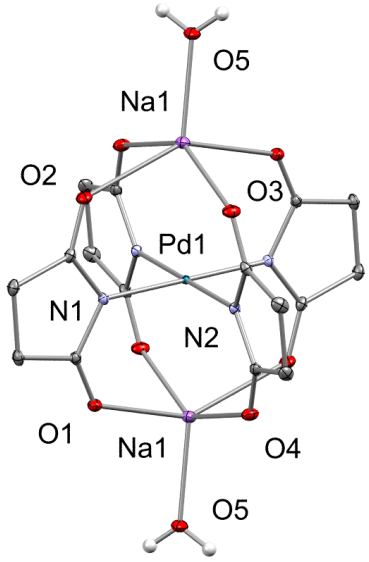

Figure S30. Thermal ellipsoid plot showing $\mathbf{3^{Na}}$ at 50% probability. H atoms (except on H_2O), lattice water, and disorder in coordinated H_2O (O5) are omitted.

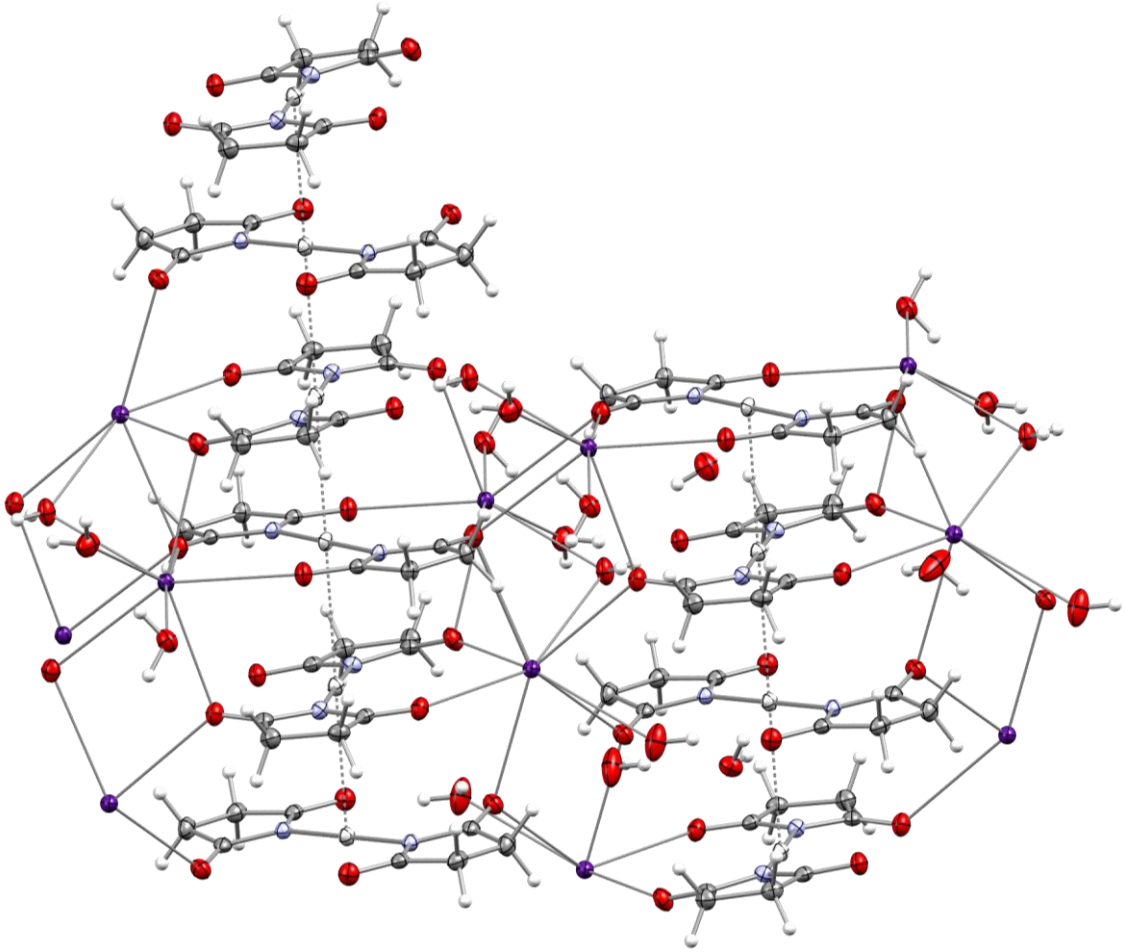

Figure S31. Thermal ellipsoid plot showing section of polymeric $Cs[Ag(succ)_2] \cdot 4\ H_2O$ ($\mathbf{1^{Cs}}$) at 50% probability.

10: Powder X-ray Diffraction

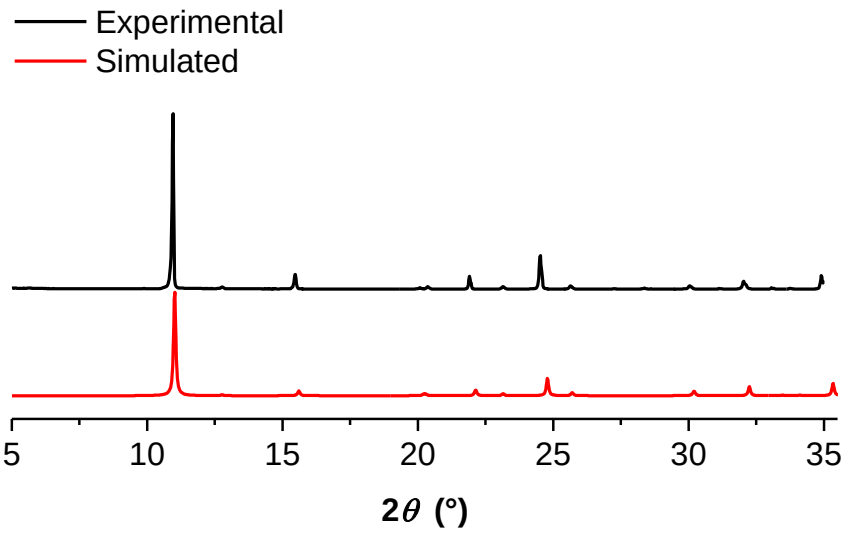

Figure S32. Powder X-ray diffraction pattern of **2**^{Cs} (room temperature); the simulation is based on the structure from single crystal X-ray diffraction at 122(2) K. Intensities are in arbitrary units.

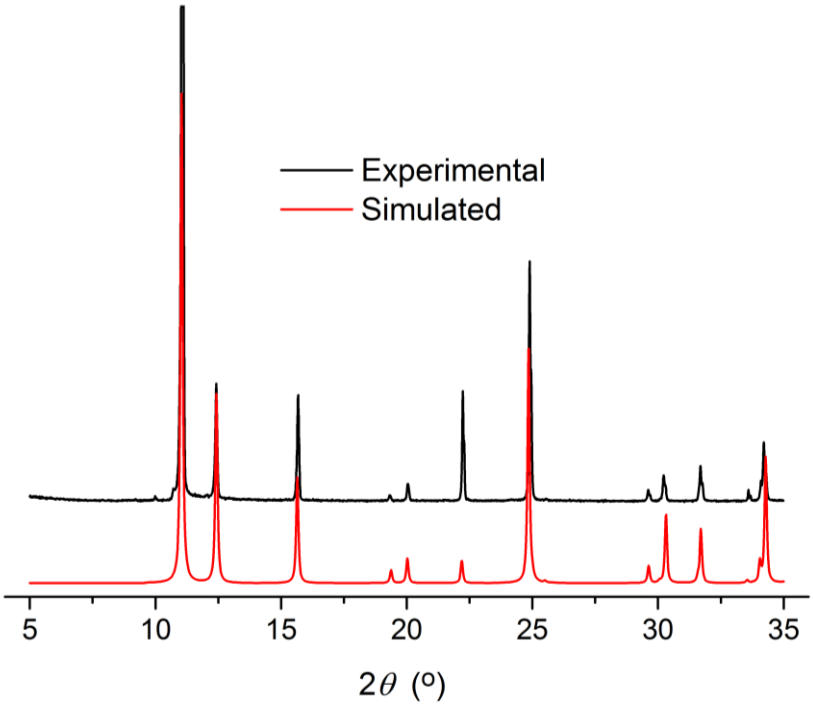

Figure S33. Powder X-ray diffraction pattern of **2**^{Ag} (room temperature); the simulation is based on the structure from single crystal X-ray diffraction at 122(2) K. Intensities are in arbitrary units.

11: Magnetic Measurements

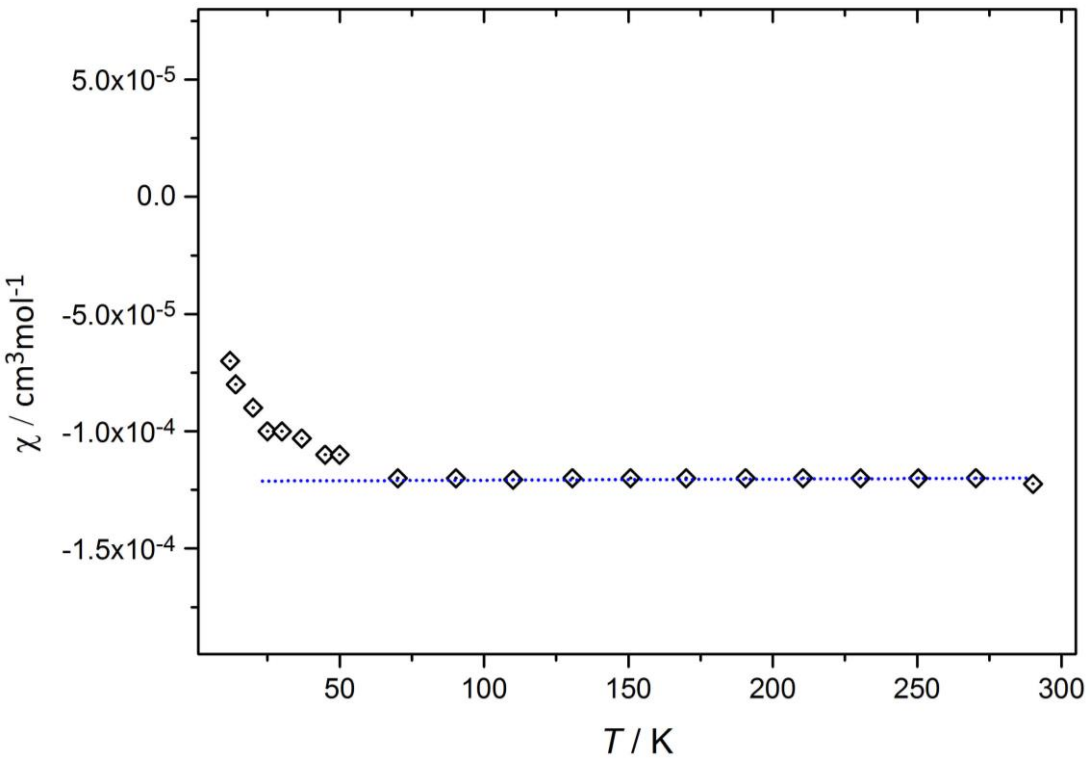

Figure S34. DC SQUID magnetometric measurements of $\mathbf{2^{Cs}}$.

12: Computational modeling

Density Functional Theory (DFT) calculations were performed with version 5.0.3 of the ORCA software package.[9] Single point energies were calculated using the B3LYP functional, the def2-TZVPP basis,[10] and employing crystallographic coordinates without any modelling of lattice effects. Transition energies and intensities were calculated by TDDFT isolating the 30 lowest roots using the same basis sets and functional as the single point calculations. Integration grid accuracy was ORCA standard defgrid2 yielding 246176 grid points.

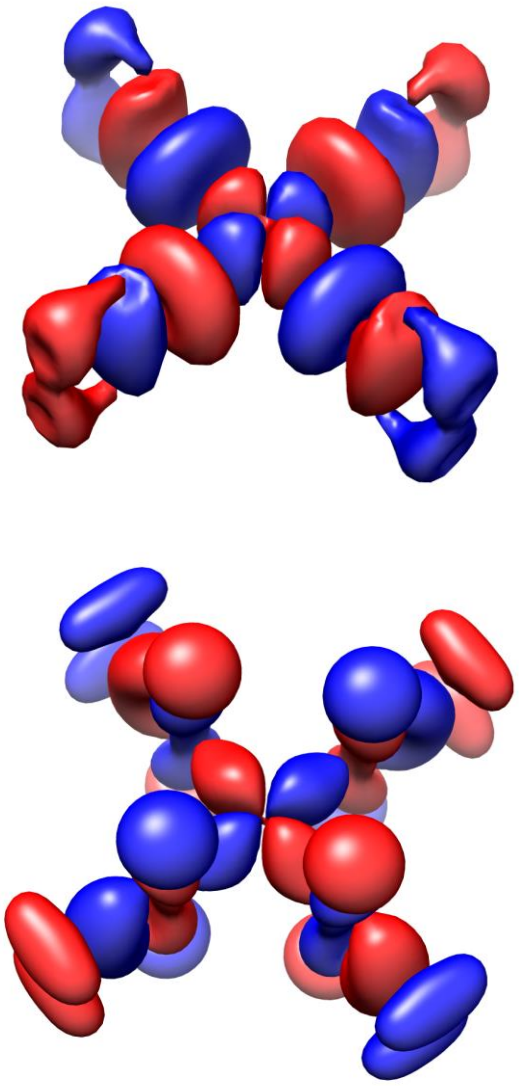

Figure S35. Sigma interaction orbitals for **2**^{Rb}. Top: LUMO orbital with ca. 35% Ag character. Bottom: filled sigma bonding orbital with ca. 12% Ag character (HOMO -5.5 eV).

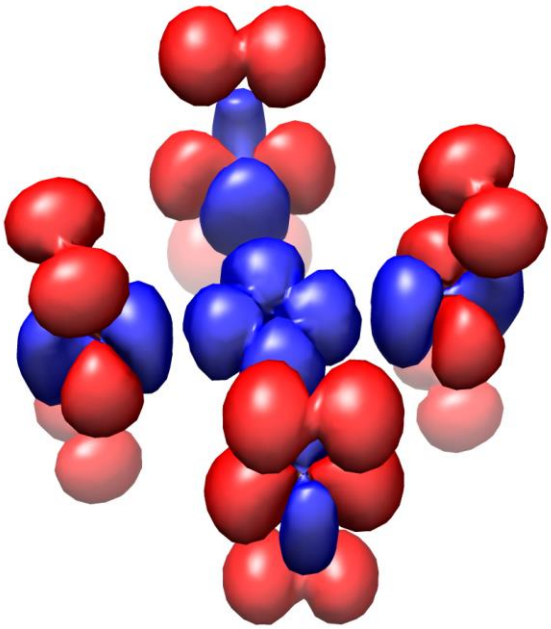

Figure S36. TDDFT calculated transition density change for the most intense electric dipole transition of $\mathbf{2^{Rb}}$ (346 nm). Blue: density increase; Red: electron density depletion. Excitation is into MO #120 (LUMO) with appreciable Ag character from mostly ligand-based MOs.

13: References

1. G. R. Fulmer, A. J. M. Miller, N. H. Sherden, H. E. Gottlieb, A. Nudelman, B. M. Stoltz, J. E. Bercaw and K. I. Goldberg, *Organometallics*, 2010, **29**, 2176-2179.
2. A. Bielecki and D. P. Burum, *J. Magn. Reson. Ser. A*, 1995, **116**, 215-220.
3. J. Skibsted, N. C. Nielsen, H. Bildsøe and H. J. Jakobsen, *Chem. Phys. Lett.*, 1992, **188**, 405-412.
4. *Bruker; Bruker AXS, Inc. SAINT, Version 7.68A; Bruker AXS: Madison, WI, 2009.*
5. G. Sheldrick, *SADABS, Version 2008/2; University of Göttingen: Germany, 2003.*
6. (a) O. V. Dolomanov, L. J. Bourhis, R. J. Gildea, J. A. K. Howard and H. Puschmann, *J. Appl. Crystallogr.*, 2009, **42**, 339-341; (b) L. J. Bourhis, O. V. Dolomanov, R. J. Gildea, J. A. K. Howard and H. Puschmann, *Acta Crystallogr., Sect. A*, 2015, **71**, 59-75.
7. G. Sheldrick, *Acta Crystallogr., Sect. A*, 2008, **64**, 112-122.
8. (a) R. Mason, *Acta Cryst.*, 1961, **14**, 720-724; (b) M. Yu, X. Huang and F. Gao, *Acta Crystallogr., Sect. E*, 2012, **68**, o2738.
9. a) F. Neese, The ORCA Program System. Wiley *Interdiscip. Rev.:Comput. Mol. Sci.* 2012, **2**, 73−78. b) F. Neese, ; F. Wennmohs, ; U. Becker, C. Riplinger, *J. Chem. Phys*. 2020, **152**, 224108.
10. F. Weigend, R. Ahlrichs, *Phys. Chem. Chem. Phys*. 2005, 7, 3297.